ACS ENVIRONMENTAL Au
AN OPEN ACCESS JOURNAL OF THE AMERICAN CHEMICAL SOCIETY

Editors' Choice
Open Access

pubs.acs.org/environau

Article

Bioaccumulation Dynamics of Metal Ions and Complexes by Aquatic Organisms: An Extended Best and Michaelis–Menten Framework for the Interplay between Chemodynamics, Bioavailability, and Biouptake Kinetics

Jérôme F. L. Duval,* Herman P. van Leeuwen, and Raewyn M. Town

Cite This: https://doi.org/10.1021/acsenvironau.5c00293

Read Online

ACCESS | Metrics & More | Article Recommendations | Supporting Information

ABSTRACT: This study elaborates a theoretical framework to understand metal bioaccumulation beyond the limitations of the equilibrium-based Biotic Ligand Model (BLM). By integrating the dynamics of metal speciation in aquatic media with the kinetics of metal biouptake, the formalism predicts metal bioavailability under conditions where the BLM fails, such as high degrees of metal complexation, diffusion-limited metal uptake, and/or internalization of intact metal complexes. The theory accounts for the reactive transport of free metal ions and complexes, incorporating different uptake mechanisms by facilitated and passive diffusion. Extended Best expressions are derived for the flux of metal biouptake by coupling extracellular metal chemodynamics (intertwined diffusion and complexation) with Michaelis–Menten uptake kinetics. The approach provides a unified rationale for various bioaccumulation situations, including the uptake of lipophilic complexes, and the concomitant uptake of free and complexed metals through distinct or shared diffusion-facilitated pathways with competitive, noncompetitive, and/or uncompetitive inhibitions. Computational examples are detailed to illustrate the intricate interplay between metal species transport dynamics and biouptake kinetics for all bioaccumulation cases, particularly addressing how the metal internalization flux is impacted by the (bioavai)lability of metal complexes, whether or not they are internalized intact. The benefits of the formalism are further illustrated through an analysis of well-characterized experimental data on neodymium (Nd) uptake by *Chlamydomonas reinhardtii* in the absence/presence of well-defined organic ligands. This analysis not only derives key metal biouptake and bioaffinity parameters but also provides solid evidence of the BLM's failure to describe the data. The quantitative interpretation of Nd bioaccumulation data leads to the identification of two potential uptake mechanisms, and a methodology to distinguish between them is discussed. Overall, this work establishes a more accurate and comprehensive theoretical foundation for predicting metal bioaccumulation in aquatic systems, thereby fundamentally challenging the common equilibrium-based perception of metal bioavailability.

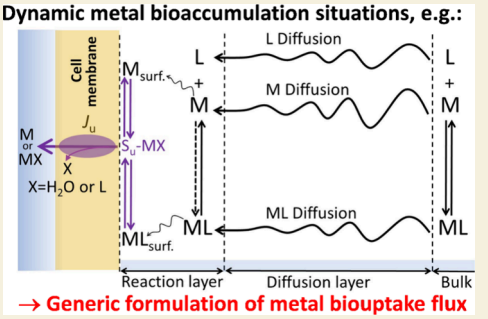

KEYWORDS: *metal speciation, metal bioaccumulation, chemical kinetics, diffusion, competitive inhibition, BLM, rare earth metals*

1. INTRODUCTION

The bioavailability of metal ions depends on their chemical speciation, i.e., their distribution over different physicochemical forms such as the free (hydrated) metal ion and the complexes it forms with various inorganic and organic ligands (L). Generally, the free metal ion (M) is the bioreactive (i.e., internalizable) metal form with few exceptions, e.g., lipid soluble metal complexes are proposed to cross biological membranes intact by passive diffusion.[1,2] Biouptake of metal ions involves (i) their diffusion toward the biological interface (biointerface in short), (ii) their association with a biological ion transporter, followed by (iii) their internalization. Depending on the relative magnitudes of the diffusive supply flux of free metal ions from the medium toward the biointerface and the metal internalization flux, a gradient in the free metal ion concentration may be established on the external medium side of the biointerface. The presence of a gradient in free metal ion concentration provides a driving force for the dissociation of metal complexes (ML), which buffers the diffusive supply flux of free M to an extent determined by the so-called lability of ML on the time scale of biouptake.[3,4] Thus, the bioavailability and bioaccumulation kinetics of metal ions are governed by the interplay between chemical speciation dynamics in the exposure medium and the time scale of processes occurring at the biological interface and within the organism. Various

Received: November 27, 2025
Revised: April 1, 2026
Accepted: April 1, 2026

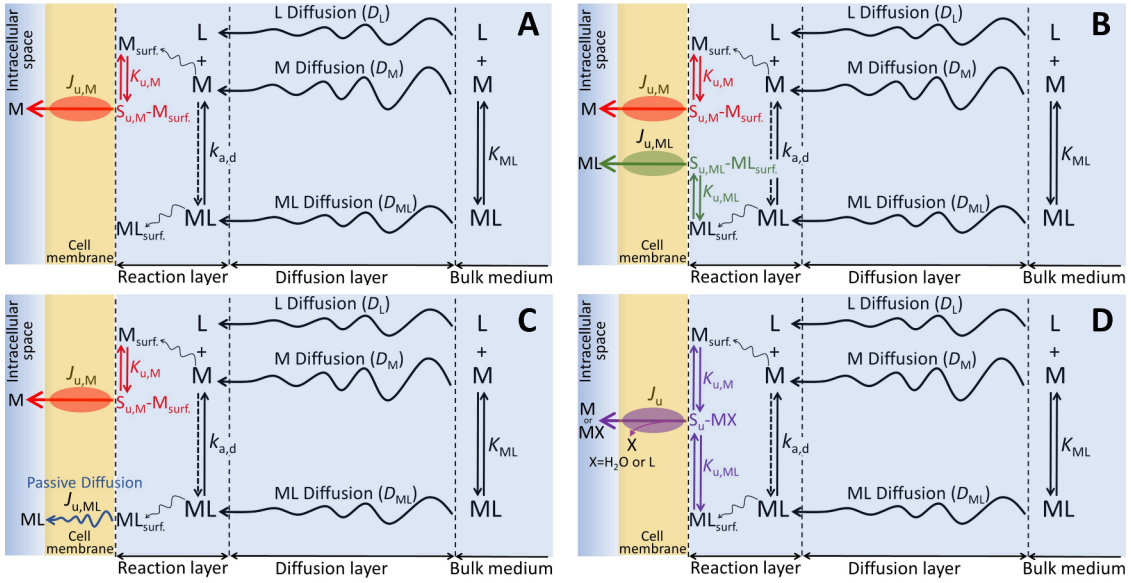

Figure 1. Schematic illustrations of the bioaccumulation scenarios considered here for the uptake of free metal (M) and/or complexed metal (ML), and representation of the interplay between the kinetics of the complexation reaction M + L ↔ ML and the diffusion of M and ML from the bulk medium to the surface of the metal-consuming organism. (A) Uptake of M via a facilitated diffusion pathway. (B) Uptake of M and ML via two separate facilitated diffusion pathways. (C) Uptake of M and ML via a facilitated diffusion pathway and a passive diffusion route, respectively. (D) Uptake of M and ML via a single facilitated diffusion pathway and occurrence of inhibition processes between M and ML along the lines detailed in Figure 2. $S_{u,M}$ and $S_{u,ML}$ represent the internalization sites for M and ML, respectively, while S_u corresponds to the internalization sites operational for both M and ML species. More specifically, $S_{u,M}$ and $S_{u,ML}$ are the active sites of the protein ensuring the translocation of M and ML across the biological barrier (cell membrane), respectively. See text for further details.

metal bioaccumulation scenarios are shown schematically in Figure 1, and all of them underpin a possible contribution of metal complexes to metal bioavailability,[2] as further detailed in this work.

Despite the inherent dependence of metal bioavailability and bioaccumulation on the kinetics of metal complexation and time scales of diffusion and biouptake, there is a large body of literature which entirely disregards the dynamic nature of the involved processes. For instance, the widely used biotic ligand model (BLM)[5,6] implicitly assumes that the diffusional supply flux of free metal ion is not rate-limiting, and the only relevant concentration of chemical species for biouptake is then the equilibrium concentration of free M in the bulk exposure medium. The free M concentration is typically computed by various equilibrium speciation models, each with their own limitations.[7] Furthermore, there is typically a paucity of information on the physicochemical properties of the involved organic ligands, which may include natural and engineered molecular and nanoparticulate complexants.[8−10] It has been shown that the assumption that only the free M is involved in biouptake is valid only if the diffusive flux of free M (*unsupported* by coupled transport of labile complex species) is much greater than the biouptake flux.[3,11−15] This dynamic condition may be rather severe under typical conditions in aquatic ecosystems, e.g., those with a high degree of metal complexation, and particularly so in the presence of nanoparticulate complexes.[16−18] In making the connection between biouptake and toxicity, the BLM assumes that toxicity occurs once the extent of metal ion binding to so-called "biotic ligands" exceeds a certain threshold level, irrespective of the time scale.[5,6]

Within BLM-type frameworks, the influence of various factors such as pH and dissolved organic carbon on metal ion bioavailability and toxicity is considered in terms of their effects on the equilibrium concentration of the free metal ion in the bulk exposure medium and equilibrium competition for association with the biotic ligands. This disregard of dynamic factors likely underpins the need for inclusion of many empirical factors and recalibration of the BLM to fit experimental observations for each organism and for each exposure condition considered.[19] The observation that fully empirical multiple linear regression models perform as well as—or better than—BLM for predictions of metal bioavailability and potential toxicity underscores the shortcomings of the BLM approach.[20,21]

Herein we elaborate a comprehensive theoretical framework to describe a range of metal bioaccumulation scenarios where the bioavailability of M may not conform to the standard BLM equilibrium predictions. In detail, the processes considered include the interplay between the reactive transfer of metal ions and metal complexes—termed hereafter as metal *chemodynamics*, ruled by metal diffusion transport and complexation reaction kinetics—toward the surface of a metal-consuming organism (biointerface), and the bioaccumulation of M and/or ML via different uptake pathways, i.e., facilitated and/or passive diffusion routes with or without competitive inhibition between M and ML (Figure 1). In all cases involving facilitated diffusion, the relevant kinetics of metal translocation process across the biological membrane is derived from the Michaelis−Menten mechanism.[3,22] Our findings highlight the (limited) range of kinetic conditions under which BLM-type models are applicable. They further provide a solid theoretical rationale of a large spectrum of metal bioaccumulation cases identified in literature as exceptions to the standard BLM model,[2] and never previously formulated with the proper account of intertwined metal chemodynamics and kinetics of M and/or ML biouptake. The benefits of the theory are illustrated by our detailed analysis of

https://doi.org/10.1021/acsenvironau.5c00293
ACS Environ. Au XXXX, XXX, XXX−XXX

selected experimental data taken from well-documented metal bioaccumulation literature, beyond the restrictive biouptake BLM framework and without *a priori* equilibrium-based considerations. While the theoretical framework developed herein focuses on the coupling between metal chemodynamics in solution and interfacial biouptake kinetics, it is important to recognize that biological uptake can be governed in some situations by specific membrane transport protein mechanisms. For instance, metal internalization can be influenced by ion exchange processes (symport or antiport) or the presence of required cosubstrates. Notable examples include the role of chloride as an exchange ion for copper,[23,24] or the requirement of bicarbonate for the transport of divalent metals like Zn, Mn, and Cd via ZIP8 transporters.[25,26] Although these specific biological transport pathways are not explicitly considered in the current theory, they may represent critical biological layers that - depending on the system - may complement the metal chemodynamic and bioaccumulation processes addressed in this work.

2. MATERIALS AND METHODS

Selection of Experimental Data to be Analyzed with the Here-Reported Theory. While there are numerous publications on the biouptake of metal ions by various organisms, most are not sufficiently documented for our purposes. We identified studies which provided sufficient details on the exposure medium composition and biouptake data as a function of time. These studies refer to the biouptake of neodymium[27] by the unicellular green algae *Chlamydomonas reinhardtii* in the absence or presence of organic ligands (malic acid and citric acid). For this system, the authors evidenced the failure of the standard BLM formulation for predicting metal biouptake and they invoked the bioavailability of formed complexes as a possible source of deviation between experiments and BLM computations.

3. THEORY

3.1. Setting the Stage

In the following, we consider the reactive transfer of free metal ions (M) and metal complexes (ML) from a medium containing a metal-complexing ligand (L) to the surface of a spherical metal-consuming organism with curvature radius a. We elaborate below the so-far missing expressions that define the M and ML biouptake fluxes, denoted as $J_{u,M}$ and $J_{u,ML}$ (mol m^2 s^{-1}), respectively, for the different bioaccumulation scenarios schemed in Figure 1. The approach accounts explicitly for the coupling between M/ML chemodynamics in the medium and the kinetics of the relevant M/ML interfacial biouptake processes.

In detail, we differentiate cases where the bioreactive (internalizable) metal forms are only the free metal species M (Figure 1A) from those where both M and ML can be internalized (Figures 1B–D). In the latter situation, we further distinguish scenarios where M and ML are bioaccumulated according to (i) two distinct facilitated diffusion pathways involving 2 different transporters, one for M and the other for ML (Figure 1B), (ii) a facilitated diffusion of M and a passive diffusion of ML (Figure 1C), and (iii) a single facilitated diffusion pathway mediated by one transporter type operating both for M and ML (Figure 1D). The bioaccumulation scenarios pictured in Figure 1 cover the situations denoted as *Type 1* to *Type 5* by Zhao et al.[2] (cf. Figure 2 therein) and qualified by those authors as the major exceptions to classical equilibrium models when predicting the bioavailability of metal complexes. Namely:

- *Type 1*-situation is that where there is passive diffusion of lipophilic metal complexes. It corresponds to the case sketched in Figure 1C in the limit where there is no uptake of free M, i.e., $J_{u,M} = 0$. Examples include the uptake by fish[28] and algae[29] of complexes formed between Cd^{2+}, Ni^{2+}, and Pb^{2+} and ligands such as dithiocarbamates, xanthates, dialkyldithiophosphates and pyridinethiones.
- *Type 2*-situation is that where there is uptake of hydrophilic metal complexes through a ligand transporter system. It corresponds to the case sketched in Figure 1B in the limit $J_{u,M} = 0$. Examples include the uptake of Cd-citrate complexes by the unicellular algae *Pseudokirchneriella subcapitata*,[30] or the uptake of Ag through the $S_2O_3^{2-}$ transport system by *Chlamydomonas reinhardtii*.[31]
- *Type 3*-situation is that where there is reaction of a complex ML with a biotic ligand at the cell surface and the ensuing formation of a so-called ternary complex. It corresponds to the case sketched in Figure 1D in the limit $J_{u,M} = 0$, with the ternary complex being formed between the active site of the protein transporter, S_u, and the complex ML. Examples include the uptake of Sc^{3+} by *C. reinhardtii* above pH 6.5.[32]
- *Type 4*-situation represents an example where labile metal complexes can contribute to metal uptake (in the case of mass-transport limitation). It corresponds to the dynamic limit in Figure 1A where the rates of formation/dissociation of (fully labile) ML are fast on the effective time scale of their (slow) diffusion from the bulk medium to the surface of the organism. Examples include the uptake of Cu^{2+} by periphyton in the presence of NTA (nitrilotriacetic acid).[33]
- *Type 5*-situation represents the situation where metal exchange between the medium and biotic ligand is rate-limiting. It refers to the case where equilibrium between free M and the biotic ligand occurs on a comparable, or slower, time scale as that of the internalization step. It thus corresponds to the kinetic limit in Figure 1A, where free M features a slow formation/dissociation kinetics with the biotic ligand on the effective time scale of their (fast) diffusion from the bulk medium to the surface of the organism. Examples are rare due to the difficulty to distinguish experimentally between the situation where metal uptake is under kinetic control and the one where the uptake is thermodynamically controlled (BLM). A famous illustration is Fe uptake by two species of marine phytoplankton.[34]

It is stressed that the above classification found in literature is generally based on evaluating the ratio between the (theoretical) diffusional flux of free M and the (measured) M biouptake flux, and the use of the Michaelis–Menten equation involving or not competitive M-ML equilibrium surface adsorption. In turn, the interpretation of biouptake flux data never fully integrates the interplay between chemodynamics and biouptake kinetics of M and/or ML with the proper level of rigor. Here we present a theoretical framework with explicit expressions of the associated fluxes, which enables rigorous interpretation of the involved processes.

In Figure 1, steady-state metal transport at the organism/medium interface is rapidly achieved (within ~ ms) for organisms whose size a is of the order of 1 to 10 μm, e.g.,

https://doi.org/10.1021/acsenvironau.5c00293
ACS Environ. Au XXXX, XXX, XXX–XXX

bacteria, microalgae or consuming organs of invertebrates such as gills in fish.[3,4,12,13] In the bulk medium, far from the biological metal-consuming surface, equilibrium between M, ML and L is maintained, and their respective bulk concentrations, denoted as $c^*_{i=\mathrm{M,L,ML}}$, satisfy $K_{\mathrm{ML}} = c^*_{\mathrm{ML}}/(c^*_{\mathrm{L}}c^*_{\mathrm{M}})$ where K_{ML} ($\mathrm{m^3\ mol^{-1}}$) is the ML stability constant. In practice, there is usually an excess of L over (trace) M so that the concentration of L remains constant regardless of the advancement of the complexation reaction M + L $\rightleftarrows$ ML.[3] This legitimates the introduction of the dimensionless ML stability constant, $\overline{K}_{\mathrm{ML}}$, defined by $\overline{K}_{\mathrm{ML}} = K_{\mathrm{ML}}c^*_{\mathrm{L}}$. For the purpose of demonstration and mathematical simplification, we discard below the possible depletion of metal species from the bulk solution during bioaccumulation. The reader is referred to previous reports[12−15,35] for the modeling of such scenarios when M is the only bioreactive metal form. In addition, we assume that metal-induced toxicity effects on the biouptake processes are negligible, and we do not account for metal excretion. The former assumption is generally valid for short-term bioaccumulation and/or sufficiently low bulk metal concentrations.[3] The latter approximation is particularly applicable to organisms such as microalgae,[36] for which metal bioaccumulation data are the most extensively documented and can be analyzed by mechanistic theory. The overall process of M transfer involves the diffusion of M and ML, with diffusion coefficients $D_{i=\mathrm{M,ML}}$ ($\mathrm{m^2\ s^{-1}}$), and the interconversion kinetics between M and ML in the external aqueous medium, with association and dissociation kinetic constants k_{a} ($\mathrm{m^3\ mol^{-1}\ s^{-1}}$) and k_{d} ($\mathrm{s^{-1}}$), respectively, connected to K_{ML} by $K_{\mathrm{ML}} = k_{\mathrm{a}}/k_{\mathrm{d}}$. Meanings of symbols in this work are defined in a Glossary to ease reading. Below, we derive the expressions of the biouptake fluxes $J_{\mathrm{u},i=\mathrm{M,ML}}$ for the metal bioaccumulation scenarios shown in Figure 1. This derivation (Section 3.3) follows the evaluation in Section 3.2 of the M and ML concentration profiles in the medium, and their corresponding diffusional supply fluxes to the metal-consuming biointerface.

3.2. Expressions of M/ML Concentration Profiles and Supply Fluxes to the Organism's Metal-Consuming Surface

Herein we adopt the radial coordinate r with the origin $r = 0$ positioned at the center of the metal-consuming organism. Under the conditions outlined in Section 3.1, the spatial distributions of M and ML concentrations, denoted as $c_{\mathrm{M}}(r)$ and $c_{\mathrm{ML}}(r)$, respectively, are governed by the coupled steady-state Nernst−Planck equations corrected for the chemical terms pertaining to ML formation and dissociation kinetics

$$\begin{cases} D_{\mathrm{M}}\nabla_r^2 c_{\mathrm{M}}(r) + k_{\mathrm{d}}c_{\mathrm{ML}}(r) - k_{\mathrm{a}}c_{\mathrm{ML}}(r)c^*_{\mathrm{L}} = 0 & \text{(a)} \\ D_{\mathrm{ML}}\nabla_r^2 c_{\mathrm{ML}}(r) - k_{\mathrm{d}}c_{\mathrm{ML}}(r) + k_{\mathrm{a}}c_{\mathrm{ML}}(r)c^*_{\mathrm{L}} = 0 & \text{(b)} \end{cases} \quad (1)$$

where $\nabla_r^2 f \equiv r^{-2}\mathrm{d}(r^2\mathrm{d}f/\mathrm{d}r)/\mathrm{d}r$ is the Laplacian operator in spherical geometry with f a dummy function of the radial position r. The boundaries associated with eq 1 specify M and ML surface concentrations that hold far from- and at- the organism's surface, i.e.,

$$\begin{cases} c_{i=\mathrm{M,L,ML}}(r \to \infty) = c^*_{i=\mathrm{M,L,ML}} & \text{(a)} \\ c_{i=\mathrm{M,ML}}(r = a) = c^{(\mathrm{a})}_{i=\mathrm{M,ML}} & \text{(b)} \end{cases} \quad (2)$$

where $c^{(\mathrm{a})}_{i=\mathrm{M,ML}}$ stand for the M and ML surface concentrations. For mathematical convenience, we introduce the dimensionless M and ML concentration profiles defined by $\overline{c}_{i=\mathrm{M,ML}}(\overline{r}) = c_{i=\mathrm{M,ML}}(\overline{r})/c^*_{i=\mathrm{M,ML}}$ with $\overline{r} = r/a$ the scaled radial position, and $\varepsilon = D_{\mathrm{ML}}/D_{\mathrm{M}}$ the ML and M diffusion coefficients ratio. Following the procedure outlined in Supporting Information (SI-A), the solution of eqs 1 and 2 can be written in the concise form

$$\begin{cases} \overline{c}_{\mathrm{M}}(\overline{r}) = 1 - \dfrac{1}{\overline{r}}\left[1 - \dfrac{\overline{c}^{(\mathrm{a})}_{\mathrm{M}} + \varepsilon\overline{K}_{\mathrm{ML}}\overline{c}^{(\mathrm{a})}_{\mathrm{ML}}}{1 + \varepsilon\overline{K}_{\mathrm{ML}}} + \dfrac{\varepsilon\overline{K}_{\mathrm{ML}}}{1 + \varepsilon\overline{K}_{\mathrm{ML}}}(\overline{c}^{(\mathrm{a})}_{\mathrm{ML}} - \overline{c}^{(\mathrm{a})}_{\mathrm{M}})\mathrm{e}^{-\overline{h}_{\mathrm{a}}(\overline{r}-1)}\right] & \text{(a)} \\ \overline{c}_{\mathrm{ML}}(\overline{r}) = 1 - \dfrac{1}{\overline{r}}\left[1 - \dfrac{\overline{c}^{(\mathrm{a})}_{\mathrm{M}} + \varepsilon\overline{K}_{\mathrm{ML}}\overline{c}^{(\mathrm{a})}_{\mathrm{ML}}}{1 + \varepsilon\overline{K}_{\mathrm{ML}}} - \dfrac{1}{1 + \varepsilon\overline{K}_{\mathrm{ML}}}(\overline{c}^{(\mathrm{a})}_{\mathrm{ML}} - \overline{c}^{(\mathrm{a})}_{\mathrm{M}})\mathrm{e}^{-\overline{h}_{\mathrm{a}}(\overline{r}-1)}\right] & \text{(b)} \end{cases} \quad (3)$$

where $\overline{c}^{(\mathrm{a})}_{i=\mathrm{M,ML}} = c_{i=\mathrm{M,ML}}(\overline{r} = 1)/c^*_{i=\mathrm{M,ML}}$ refers to the dimensionless M and ML surface concentrations, and the dimensionless $\overline{h}_{\mathrm{a}}$ in eq 3 is defined by

$$\overline{h}_{\mathrm{a}} = \sqrt{\overline{\kappa}_{\mathrm{a}}(1 + \varepsilon\overline{K}_{\mathrm{ML}})/(\varepsilon\overline{K}_{\mathrm{ML}})} \quad (4)$$

In eq 4, $\overline{\kappa}_{\mathrm{a}} = k_{\mathrm{a}}a^2c^*_{\mathrm{L}}/D_{\mathrm{M}}$ is the dimensionless Damkhöler number that compares the time scale of M diffusion, a^2/D_{M}, and the ML formation time scale, $1/(k_{\mathrm{a}}c^*_{\mathrm{L}})$.[3] Equivalently, $\sqrt{\overline{\kappa}_{\mathrm{a}}}$ compares the organism radius a with the thickness $\sqrt{D_{\mathrm{M}}/(k_{\mathrm{a}}c^*_{\mathrm{L}})}$ of the reaction layer (Figure 1) which represents the distance traveled by a free M before it reassociates with L to form ML.

The diffusional supply fluxes of M and ML from the bulk solution to the surface of the metal-consuming organism, denoted as $J_{i=\mathrm{M,ML}}$, are defined by

$$J_{i=\mathrm{M,ML}} = D_{i=\mathrm{M,ML}}(\mathrm{d}c_{i=\mathrm{M,ML}}/\mathrm{d}r)|_{r=a} \quad (5)$$

Combining eqs 3 and 5, we obtain the following expressions that define $J_{i=\mathrm{M,ML}}$

$$\begin{cases} J_{\mathrm{M}}/J^{\max}_{\mathrm{Diff,M}} = 1 + \gamma_{\mathrm{M}}y - (1 + \gamma_{\mathrm{M}})x & \text{(a)} \\ J_{\mathrm{ML}}/J^{\max}_{\mathrm{Diff,ML}} = 1 + \gamma_{\mathrm{ML}}x - (1 + \gamma_{\mathrm{ML}})y & \text{(b)} \end{cases} \quad (6)$$

where we have written the dimensionless M and ML surface concentrations in the concise forms $x = \overline{c}^{(\mathrm{a})}_{\mathrm{M}}$ and $y = \overline{c}^{(\mathrm{a})}_{\mathrm{ML}}$, and we have further introduced $J^{\max}_{\mathrm{Diff},i=\mathrm{M,ML}}$ the maximum M and ML diffusion fluxes from bulk solution to the organism's surface, defined by $J^{\max}_{\mathrm{Diff},i=\mathrm{M,ML}} = D_{i=\mathrm{M,ML}}c^*_{i=\mathrm{M,ML}}/a$, which is

https://doi.org/10.1021/acsenvironau.5c00293
ACS Environ. Au XXXX, XXX, XXX−XXX

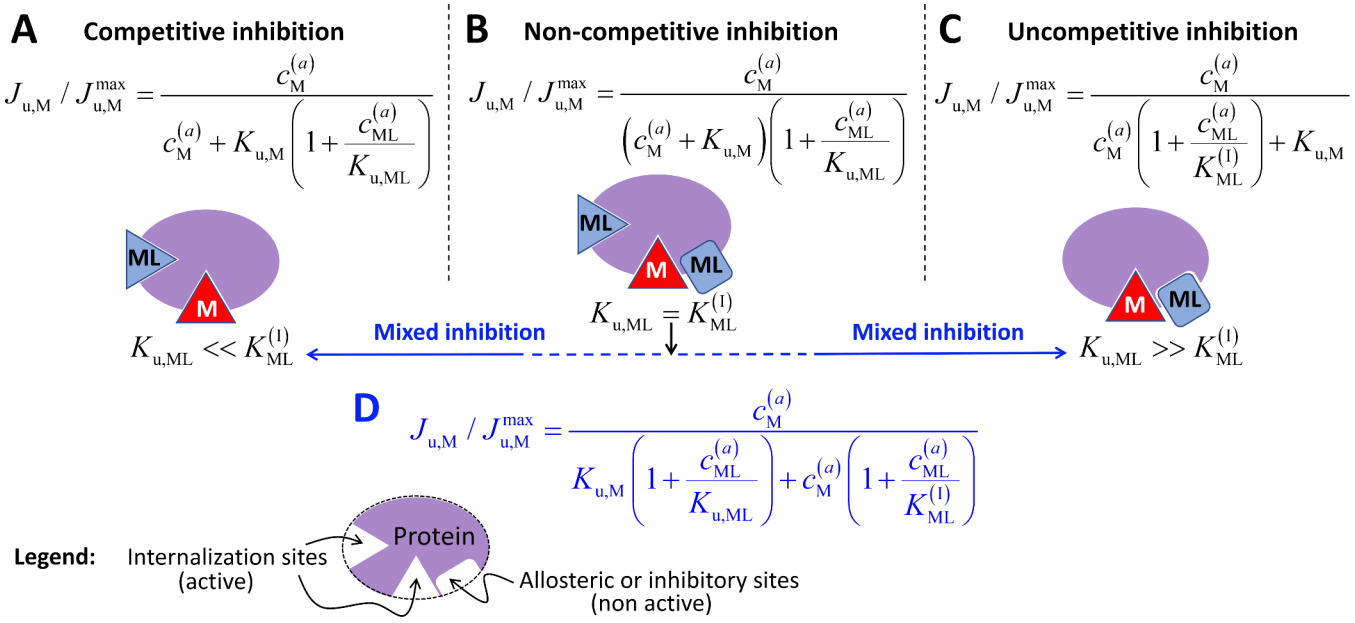

Figure 2. Expressions of the normalized M uptake flux, $J_{u,M}/J_{u,M}^{max}$, for the bioaccumulation scenario sketched in Figure 1D in the case of (A) M/ML competitive inhibition, (B) M/ML noncompetitive inhibition, and (C) M/ML uncompetitive inhibition. The expression of $J_{u,M}/J_{u,M}^{max}$ for a mixed inhibition process is provided in (D) (blue font). The characteristic half-saturation constants $K_{u,i=M,ML}$ and $K_{i=M,ML}^{(I)}$ (mol m^{-3}) refer to the reciprocals of the stability constants (m^3 mol^{-1}) that describe the M and ML binding with their respective active and inhibitory transporter sites, respectively. The M and ML concentrations at the surface of the metal-consuming organism are denoted as $c_{i=M,ML}^{(a)}$. The competitive, noncompetitive, and uncompetitive inhibitions by ML are limits of the mixed inhibition process for $K_{u,ML} \ll K_{ML}^{(I)}$, $K_{u,ML} = K_{ML}^{(I)}$, and $K_{u,ML} \gg K_{ML}^{(I)}$, respectively. For the sake of conciseness, only the expressions of $J_{u,M}/J_{u,M}^{max}$ are given here. Formulations of $J_{u,ML}/J_{u,ML}^{max}$ for the various inhibition scenarios of interest derive from those of $J_{u,M}/J_{u,M}^{max}$ after inverting the 'M' and 'ML' notations in all of the involved symbols. The dimensionless expressions defining the metal biouptake fluxes relevant for the various scenarios pictured in this figure are defined in Section 3.3. See text for further details.

achieved when $\overline{c}_M^{(a)} = 0$. Equation 6 involves the dimensionless parameters $\gamma_{i=M,ML}$ given by $\gamma_{ML} = \gamma_M/(\varepsilon\overline{K}_{ML}) = \overline{h}_a/(1 + \varepsilon\overline{K}_{ML})$, where $\overline{h}_a$ is defined by eq 4. These parameters describe how the coupling between M complexation kinetics and M/ML diffusions (Figure 1) impact the supply fluxes $J_{i=M,ML}$ at given M and ML surface concentrations. Using eq 4, the parameters $\gamma_{i=M,ML}$ can be rewritten in the convenient forms

$$\begin{cases} \gamma_M = \sqrt{\varepsilon\overline{K}_{ML}\overline{\kappa}_a/(1 + \varepsilon\overline{K}_{ML})} & \text{(a)} \\ \gamma_{ML} = \sqrt{\overline{\kappa}_a/[\varepsilon\overline{K}_{ML}(1 + \varepsilon\overline{K}_{ML})]} & \text{(b)} \end{cases} \quad (7)$$

3.3. Expressions of the M and ML Biouptake Fluxes

For all bioaccumulation scenarios shown in Figure 1, steady-state metal transport imposes that the M and ML biouptake fluxes, $J_{u,i=M,ML}$, must fulfill the following condition

$$J_{u,i=M,ML} = J_{i=M,ML} \quad (8)$$

where the M and ML diffusional supply fluxes, $J_{i=M,ML}$, are defined by eqs 6 and 7. Consistent with literature, we assume that facilitated M and/or ML diffusion—when operational—proceeds according to the Michaelis–Menten mechanism.[3,22] This involves a rapid adsorption of the bioreactive M and/or ML at the corresponding M and/or ML internalization sites (denoted as $S_{u,M}$ and $S_{u,ML}$ in Figure 1, representing the active sites of the M and ML protein transporters, respectively). This fast adsorption is then followed by a rate-limiting translocation of M and/or ML across the biological barrier, with kinetic constant $k_{int,M}(s^{-1})$ and $k_{int,ML}(s^{-1})$, respectively. Using an analogy to the well-established inhibition principles described by Michaelis–Menten enzyme kinetics theory,[22,37] we can further categorize the bioaccumulation scenario depicted in Figure 1D. Specifically, we distinguish between cases involving M-ML competitive inhibition, noncompetitive inhibition, uncompetitive inhibition and mixed inhibition. Considering the inhibition of M uptake by ML for the sake of demonstration, Figure 2 illustrates each of these inhibition processes, clarifying how M and ML bind to the active (internalization) and/or nonactive (inhibitory) sites on the protein transporter that facilitates M translocation across the biological barrier.

The expressions for M and ML biouptake fluxes are derived below for each bioaccumulation scenario shown in Figures 1 and 2, starting with the case where M is the only bioreactive metal form (Figure 1A).

3.3.1. Case Where M Is the Only Bioreactive Metal Form (Figure 1A). In this situation where ML is not internalized, the only relevant biouptake flux is that of the free metal species M, $J_{u,M}$. This flux depends on the (dimensionless) surface concentration of free M, $x = \overline{c}_M^{(a)}$, according to

https://doi.org/10.1021/acsenvironau.5c00293
ACS Environ. Au XXXX, XXX, XXX−XXX

the Michaelis–Menten expression written in the dimensionless format[3,12,13]

$$J_{u,M}/J_{u,M}^{max} = x/(a_M + x) \quad (9)$$

where we recall that $J_{u,M}^{max}$ is the maximum M biouptake flux. In eq 9, a_M corresponds to the dimensionless metal bioaffinity parameter given by $a_M = K_{u,M}/c_M^*$, where $K_{u,M}$ (mol m^{-3}) is the characteristic M half-saturation constant. The latter corresponds to the reciprocal of the stability constant (in m^3 mol^{-1}) that describes the binding of M with the active M-transporter sites at the cell membrane. Accordingly, a very *high* bioaffinity of M for the M-internalization sites corresponds to very *low* values of a_M or $K_{u,M}$. In the extreme $a_M \ll 1$, all M internalization sites are occupied by M (full coverage), and the limit $J_{u,M} \to J_{u,M}^{max}$ is reached. It can be verified that $J_{u,M}^{max}$ depends on $K_{u,M}$ via $J_{u,M}^{max} = K_{H,M}k_{int,M}K_{u,M}$, where $K_{H,M}$ (m) is the Henry constant for the fast M adsorption on the M internalization sites.[14] Substituting in eq 8 the expressions of $J_{u,M}$ and J_M defined by eqs 9 and 6, respectively, and further applying the condition $J_{ML} = 0$ which reflects the absence of ML internalization with J_{ML} defined by eq 6, we obtain after some algebra the following expressions for the M and ML surface concentrations $x = \overline{c}_M^{(a)}$ and $y = \overline{c}_{ML}^{(a)}$

$$\begin{cases} x = \dfrac{1}{2}(1 - a_M - b_M + (1 + a_M + b_M)\times \\ \qquad \sqrt{1 - \dfrac{4b_M}{(1 + a_M + b_M)^2}}\Big) & \text{(a)} \\ y = (1 + \gamma_{ML}x)/(1 + \gamma_{ML}) & \text{(b)} \end{cases} \quad (10)$$

Substituting eq 10 in eq 9, we derive the following dimensionless expression for the M biouptake flux

$$Q_M = \frac{1}{2}\left(\frac{1 + a_M + b_M}{b_M}\right)\left(1 - \sqrt{1 - \frac{4b_M}{(1 + a_M + b_M)^2}}\right) \quad (11)$$

where $Q_M = J_{u,M}/J_{u,M}^{max}$ is the M biouptake flux $J_{u,M}$ normalized by the maximum biouptake flux, $J_{u,M}^{max}$. Equation 11 is similar in form to the original equation developed by Best and is corrected here to account for metal speciation and ML lability (cf. eqs 12 and 13 below).[3,38,39] This corrected equation aligns with van Leeuwen's findings.[3] In eqs 10 and 11, the term b_M represents the dimensionless M bioconversion capacity. It is defined by $b_M = J_{u,M}^{max}/(pJ_{Diff,M}^{max})$ and it thus compares the maximum M biouptake flux, $J_{u,M}^{max}$, with the maximum diffusional supply flux of M at the organism surface, $J_{Diff,M}^{max}$. It also includes a dimensionless correction factor, p ($\geq$1), that specifies the contribution of ML to the overall M diffusion flux. This parameter p is defined according to[3,4]

$$p = 1 + \varepsilon\overline{K}_{ML}\xi \quad (12)$$

where ξ is the so-called ML lability index with values between 0 and unity, defined by[3,4,38]

$$\xi = \sqrt{\overline{\kappa}_a}/(\sqrt{\overline{\kappa}_a} + \sqrt{\varepsilon\overline{K}_{ML}}\sqrt{1 + \varepsilon\overline{K}_{ML}}) \quad (13)$$

The limit $\xi \to 1$ corresponds to fully labile ML complexes, i.e., complexes whose formation/dissociation kinetics are sufficiently fast on the time scale of their diffusion toward the surface of the M-consuming organism for equilibrium to be maintained between M and ML at every spatial scale. The case of nonlabile ML complexes applies when M bioaccumulation is dictated by the diffusion of free M plus the kinetics of ML dissociation at the organism surface. In this latter situation, ξ and p reduce to $\xi \to \sqrt{\overline{\kappa}_a}/(\varepsilon\overline{K}_{ML})$ and $p \to 1 + \sqrt{\overline{\kappa}_a}$, respectively.[3,4] These extremes of fully labile and nonlabile ML complexes, with diffusion- and kinetic-controlled ML contributions to the bioupake flux, respectively, refer to so-called *dynamic* complexes, i.e., systems for which the characteristic lifetimes of M and ML (given by $1/(k_a c_L^*)$ and $1/k_d$, respectively) are fast compared to the time scale $\tau_{SS} = a^2/D_M$ for establishment of steady-state diffusion of M from the medium to the M-consuming biological surface, i.e., $k_a c_L^* \tau_{SS} \gg 1$ and $k_d\tau_{SS} \gg 1$. ML systems in line with the conditions $k_a c_L^* \tau_{SS} \ll 1$ and $k_d\tau_{SS} \ll 1$ are qualified as *inert* as they do not contribute, in any manner, to the M biouptake flux. For these systems, we have $p = 1$ or, equivalently, $\xi = 0$. The reader is referred to previous reports for further details on the differentiations between inert, dynamic, labile and nonlabile ML complexes.[3,4] In particular, it can be shown that the conditions of nonlability and full lability of ML are met for $1 \ll \overline{\kappa}_a \ll \varepsilon\overline{K}_{ML}(1 + \varepsilon\overline{K}_{ML})$ and $\overline{\kappa}_a \gg \varepsilon\overline{K}_{ML}(1 + \varepsilon\overline{K}_{ML})$, respectively.[3,4,38] It is emphasized that ML complexes contributing to M biouptake (to an extent that depends on their lability) can be termed as bioavailable even though ML is not a bioreactive (internalizable) form in the bioaccumulation scenario of Figure 1A.[3] As mentioned earlier, eq 11 corresponds to the standard form of the Best equation,[39,40] corrected for the contribution of ML complexes to the flux.[3,4] It is easily verified that the normalized flux $Q_M = J_{u,M}/J_{u,M}^{max}$ increases with increasing the bioaffinity of M for the internalization sites (i.e., decreasing a_M) and/or with decreasing the bioconversion capacity of the organism (decreasing b_M), with the limit $Q_M \to 1$ reached for $a_M \ll 1$ and $b_M \ll 1$. The ratio $a_M/(pb_M)$ identifies with the so-called Bosma number, denoted as Bn_M, which compares the M diffusion conductance D_M/a (m s^{-1}) and the M internalization conductance $K_{H,M}k_{int,M}$ (m s^{-1}), where we recall that $k_{int,M}$ (s^{-1}) is the M internalization kinetic constant and $K_{H,M}$ (m) is the Henry constant for the adsorption of M on the M internalization sites,[3,14,41]

$$Bn_M = a_M/(pb_M) = a^{-1}D_M/(K_{H,M}k_{int,M}) \quad (14)$$

where the second equality is derived using the relationship $J_{u,M}^{max} = K_{H,M}k_{int,M}K_{u,M}$. In the limit $1/Bn_M \ll 1$, M bioaccumulation is kinetically limited by the internalization of M via translocation across the organism surface.[4,14,15,41] This specific situation corresponds to that tackled by the commonly accepted and applied Biotic Ligand Model (BLM). In the other extreme $1/Bn_M \gg 1$, M internalization kinetics is so fast that the rate of M bioaccumulation becomes solely determined by metal diffusion transport in the external medium. For intermediate scenarios satisfying $Bn_M \sim 1$, both internalization

https://doi.org/10.1021/acsenvironau.5c00293
ACS Environ. Au XXXX, XXX, XXX−XXX

kinetics and M diffusion—supported or not by ML diffusion depending on ML lability—define the overall kinetics of M accumulation by the organism.

In the Henry bioaccumulation regime achieved for sufficiently low bioaffinity of M, i.e., $a_M = K_{u,M}/c_M^* \gg 1$, the coverage of the internalization sites by M is well below unity and linearization of eq 9 then leads to $J_{u,M}/J_{u,M}^{max} = x/a_M$ or, equivalently, $J_{u,M} = K_{H,M}k_{int,M}c_M^{(a)}$. Under such a condition, it is easily verified that application of eq 8 leads to the following expressions of M and ML surface concentrations

$$\begin{cases} x = 1/(1 + (pBn_M)^{-1}) & \text{(a)} \\ y = 1 + \xi(x - 1) & \text{(b)} \end{cases} \tag{15}$$

which correctly compares with the results given elsewhere[3] and with the expression of the ML lability, $\xi = 1 - y$, given in refs 4,38 under the perfect sink boundary condition defined by $x = 0$. Within the Henry bioaccumulation regime, the normalized M bioaccumulation flux Q_M defined by eq 11 then simplifies into

$$Q_M = a_M^{-1}/(1 + (pBn_M)^{-1}) \tag{16}$$

which also agrees with previous findings.[3]

3.3.2. Cases Where Both M and ML Are Bioreactive Metal Forms. *3.3.2.1. Scenario Where M and ML Are Internalized by Different Facilitated Diffusion Pathways (Figure 1B).* Here, the M biouptake flux remains defined by eq 9, and the ML biouptake flux can be expressed by a Michaelis–Menten expression equivalent to that adopted for M, i.e.,

$$J_{u,ML}/J_{u,ML}^{max} = y/(a_{ML} + y) \tag{17}$$

where $J_{u,ML}^{max}$ is the maximum ML biouptake flux. In eq 17, a_{ML} is the dimensionless ML bioaffinity parameter defined by $a_{ML} = K_{u,ML}/c_{ML}^*$, where $K_{u,ML}$ (mol m^{-3}) is the ML half-saturation constant corresponding to the reciprocal of the ML binding constant with ML-internalization sites at the cell surface. The bioaffinity parameter a_{ML} is analogous to a_M defined for free metal M in eq 9, Section 3.3.1. Applying the steady-state condition $J_{u,i=M,ML} = J_{i=M,ML}$ (eq 8) where $J_{i=M,ML}$, $J_{u,M}$ and $J_{u,ML}$ are defined by eqs 6, 9, and 17, respectively, we show that M and ML surface concentrations x and y, respectively, are now defined by the following coupled quadratic equations in x and y

$$\begin{cases} A_2x^2 + A_1(y)x + A_0(y) = 0 & \text{(a)} \\ B_2y^2 + B_1(x)y + B_0(x) = 0 & \text{(b)} \end{cases} \tag{18}$$

where A_2 and B_2 are constants, and $A_{0,1}(y)$ and $B_{0,1}(x)$ are functions of y and x, respectively, given by

$$\begin{cases} \begin{bmatrix} A_0(y) \\ A_1(y) \\ A_2 \end{bmatrix} = \begin{bmatrix} -(1 + \gamma_M y) \\ 1 + \gamma_M + Bn_M^{-1} - a_M^{-1}(1 + \gamma_M y) \\ a_M^{-1}(1 + \gamma_M) \end{bmatrix} & \text{(a)} \\ \begin{bmatrix} B_0(x) \\ B_1(x) \\ B_2 \end{bmatrix} = \begin{bmatrix} -(1 + \gamma_{ML} x) \\ 1 + \gamma_{ML} + Bn_{ML}^{-1} - a_{ML}^{-1}(1 + \gamma_{ML} x) \\ a_{ML}^{-1}(1 + \gamma_{ML}) \end{bmatrix} & \text{(b)} \end{cases} \tag{19}$$

In eq 19, we have introduced the Bosma number Bn_{ML} which refers to the ML biouptake process and is the analogue of Bn_M defined by eq 14 for M. Similarly, Bn_{ML} is given by the expression

$$Bn_{ML} = a_{ML}/(pb_{ML}) = a^{-1}D_{ML}/(K_{H,ML}k_{int,ML}) \tag{20}$$

where $b_{ML} = J_{u,ML}^{max}/(pJ_{Diff,ML}^{max})$ is the ML bioconversion capacity of the organism and the counterpart of b_M for M, $k_{int,ML}$ (s^{-1}) is the ML internalization kinetic constant, and $K_{H,ML}$ (m) is the Henry constant for the ML adsorption at the ML-internalization sites. Equations 18 and 19 in x and y can be solved numerically (cf. Section 3.4) and the bioaccumulation fluxes $J_{u,i=M,ML}$ are then subsequently evaluated according to eqs 9 and 17.

Within the linear Henry regimes of M and ML bioaccumulation, applicable for $a_{i=M,ML} = K_{u,i}/c_i^* \gg 1$, the biouptake flux formulated according to eqs 9 and 17 can be linearized with respect to x and y, leading to $J_{u,M} = K_{H,M}k_{int,M}c_M^{(a)}$ and $J_{u,ML} = K_{H,ML}k_{int,ML}c_{ML}^{(a)}$. In these regimes, eqs 18 and 19 can be solved analytically, and after some developments we show that M and ML surface concentrations, x and y, are provided by the explicit expressions

$$\begin{cases} x = 1/\left\{1 + \dfrac{1 + [1 + (\eta Bn_M - 1)\xi]Bn_{ML}^{-1}}{1 + (1 - \xi)(pBn_{ML})^{-1}}(pBn_M)^{-1}\right\} & \text{(a)} \\ y = [1 + \xi(x - 1)]/[1 + (1 - \xi)Bn_{ML}^{-1}] & \text{(b)} \end{cases} \tag{21}$$

where we have introduced the dimensionless quantity $\eta = J_{Diff,ML}^{max}/J_{Diff,M}^{max} = \varepsilon\overline{K}_{ML}$ and we have given the results as a function of the ML lability index ξ (eq 13) using the relationships interconnecting $\gamma_{i=M,ML}$ and ξ

$$\begin{cases} \gamma_M = \eta\xi/(1 - \xi) & \text{(a)} \\ \gamma_{ML} = \xi/(1 - \xi) & \text{(b)} \end{cases} \tag{22}$$

which are easily obtained by combining eqs 7 and 13. In the linear Henry M and ML bioaccumulation regimes, the normalized steady-state M and ML biouptake fluxes, $Q_{i=M,ML} = J_{u,i}/J_{u,i}^{max}$, can be derived by substituting eq 21 in eq 6. After algebraic arrangements, the results read as

https://doi.org/10.1021/acsenvironau.5c00293
ACS Environ. Au XXXX, XXX, XXX−XXX

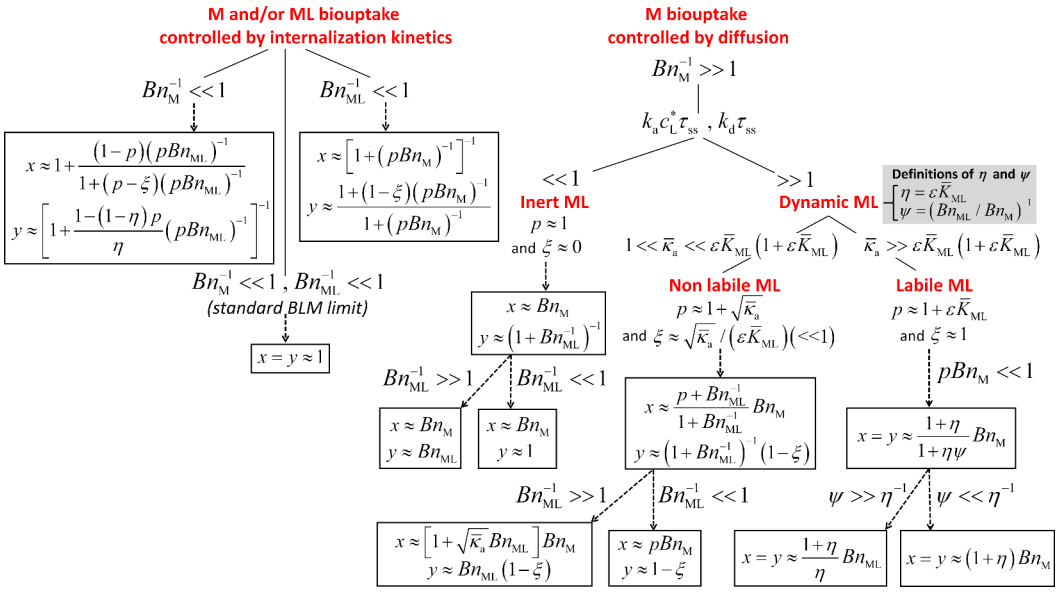

Figure 3. Limits of eq 21 defining the M and ML concentrations at the surface of the metal-consuming organism in the Henry biouptake regime (x and y, respectively) over the entire spectrum of M and ML uptake dynamic cases. Results apply here to the scenario where M and ML uptakes proceed according to different facilitated diffusion pathways (Figure 1B). The conditions for application of the standard BLM limit are specified. See text for details.

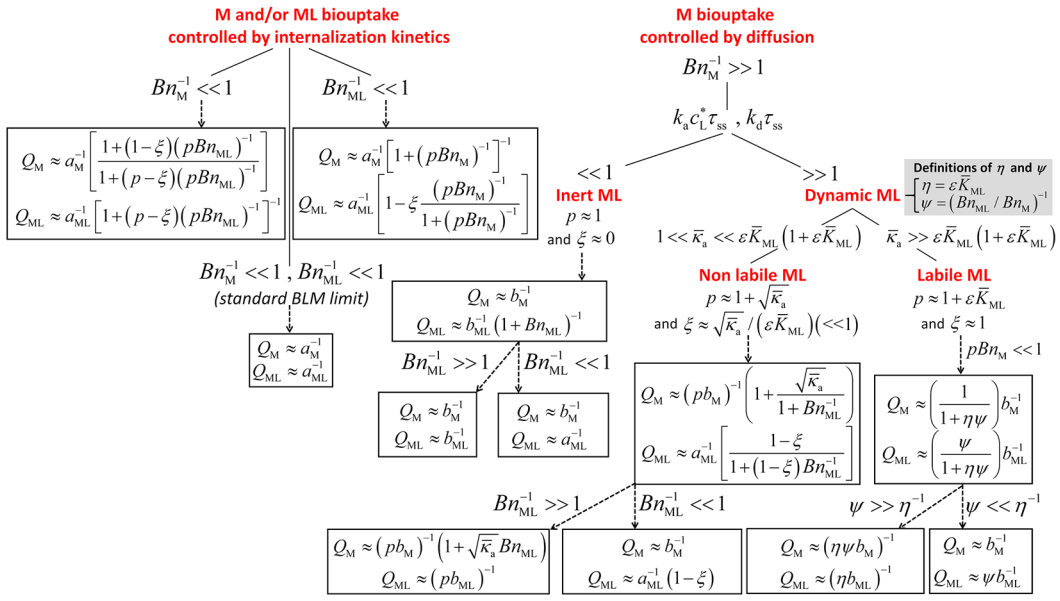

Figure 4. Limits of eq 23 defining the normalized M and ML biouptake fluxes at the surface of the metal consuming organism ($Q_M = J_{u,M}/J_{u,M}^{max}$ and $Q_{ML} = J_{u,ML}/J_{u,ML}^{max}$, respectively) in the Henry biouptake regime over the entire spectrum of M and ML uptake dynamic cases. Results apply here to the scenario where M and ML uptakes proceed according to different facilitated diffusion pathways (Figure 1B). The conditions for application of the standard BLM limit are specified. See text for details.

$$\begin{cases} Q_M = a_M^{-1} Bn_M \{1 + \dfrac{(pBn_M)^{-1}[\eta\xi + (\xi - p)\psi] - 1}{1 + (pBn_M)^{-1}\{1 + \psi[(1-\xi)(1 + Bn_M^{-1}) + \eta\xi]\}}\} & \text{(a)} \\ Q_{ML} = a_{ML}^{-1} Bn_{ML} \{1 + \dfrac{(pBn_M)^{-1}(\xi\psi - 1) - 1}{1 + (pBn_M)^{-1}\{1 + \psi[(1-\xi)(1 + Bn_M^{-1}) + \eta\xi]\}}\} & \text{(b)} \end{cases} \quad (23)$$

where we have defined the dimensionless ratio ψ which compares the relative significance of the ML and M biouptake pathways according to

$$\psi = (Bn_{ML}/Bn_M)^{-1} = a_M b_{ML}/(a_{ML} b_M) \quad (24)$$

The situation where ML is not internalized is retrieved for $k_{int,ML} \to 0$, i.e., $1/Bn_{ML} \to 0$ or, equivalently, $\psi \to 0$. Under Henry bioaccumulation conditions, it is verified that eq 23 satisfactorily reduces to $Q_{ML} \to 0$ in the limit $\psi \to 0$, while eqs 21 and 23 correctly simplify into eqs 15 and 16,

https://doi.org/10.1021/acsenvironau.5c00293
ACS Environ. Au XXXX, XXX, XXX−XXX

respectively. Most generally, it is verified that the solution of eqs 18 and 19 taken in the limit $1/Bn_{ML} \to 0$ correctly reduces to eq 10. When expressed as a function of $\gamma_{M,ML}$, the defining expressions of $Q_{M,ML}$ remain interchangeable if inverting the 'M' and 'ML' notations in all the symbols involved, regardless of the values of $a_{M,ML}$ and thus of the applicability of the Henry bioaccumulation conditions. This property is due to the inherent symmetry of eqs 6, 9, 17, 18, and 19 with respect to x and y, and 'M' and ML' symbols. The result valid in the linear Henry regime reads according to eq S5 in SI−B and it is fully equivalent to eq 23.

We provide in Figures 3 and 4 the limits of the expressions defining x, y (eq 21) and $Q_{i=M,ML} = J_{u,i}/J_{u,i}^{max}$ (eq 23), both valid in the Henry M and ML bioaccumulation regimes, across the entire spectrum of metal biouptake dynamics, i.e., when metal biouptake is controlled by M and/or ML internalization kinetics ($Bn_M^{-1} \ll 1$ and/or $Bn_{ML}^{-1} \ll 1$, respectively) or by M diffusion ($Bn_M^{-1} \gg 1$). In the latter situation, the limits of eqs 21 and 23 are derived for inert ML complexes, and for dynamic nonlabile and labile ML complexes with either internalization- or diffusion-controlled ML biouptake corresponding to $Bn_{ML}^{-1} \ll 1$ and $Bn_{ML}^{-1} \gg 1$, respectively. We stress that $Bn_{M,ML}^{-1}$ (eqs 14 and 20) reflect not only the coupling between M/ML diffusion and complexation reaction kinetics in the medium, but also some of the key properties of the metal-consuming biological surface via the involved metal bioaffinity and bioconversion parameters ($a_{i=M,ML}$ and $b_{i=M,ML}$, respectively).

3.3.2.2. Case Where M and ML Are Internalized by Facilitated and Passive Diffusions, Respectively (Figure 1C). In this scenario schemed in Figure 1C, the M uptake flux is still defined by eq 9 and the ML uptake flux can be expressed in the following operational form

$$J_{u,ML} = D_{o,ML} c_{ML}^{*} (y - y_o)/\delta_o \tag{25}$$

where $D_{o,ML}$ stands for the ML diffusion coefficient across the biological barrier of thickness δ_o, and $(y - y_o)/\delta_o$ represents the ML concentration gradient across that barrier. For the sake of simplicity, we adopt here a sink boundary at the internal side of this barrier, i.e., $y_o = 0$, which avoids the necessity to invoke the way ML species, once internalized, are handled by the organism via e.g., detoxification or storage strategies. Applying the steady-state condition $J_{u,i=M,ML} = J_{i=M,ML}$ (eq 8) where $J_{i=M,ML}$ are defined by eq 6, $J_{u,M}$ by eq 9 and $J_{u,ML}$ by eq 25, we show that M and ML surface concentrations x and y, respectively, are now defined by the algebraic equations

$$\begin{cases} A_2 x^2 + A_1 x + A_0 = 0 & \text{(a)} \\ y = \dfrac{1 + \gamma_{ML} x}{1 + \beta_{ML} + \gamma_{ML}} & \text{(b)} \end{cases} \tag{26}$$

where $A_{0,1,2}$ are all constants given here by

$$\begin{bmatrix} A_0 \\ A_1 \\ A_2 \end{bmatrix} = \begin{bmatrix} -(1 + \gamma_M + \gamma_{ML} + \beta_{ML}) \\ (1 - a_M^{-1} + Bn_M^{-1})(1 + \gamma_{ML} + \beta_{ML}) + \gamma_M(1 - a_M^{-1} + \beta_{ML}) \\ a_M^{-1}[\gamma_{ML} + (1 + \gamma_M)(1 + \beta_{ML})] \end{bmatrix} \tag{27}$$

The dimensionless parameter β_{ML} in eq 27 is defined by the ratio between the ML diffusion conductance across the biological barrier and the ML diffusion conductance from bulk solution to the outer side of the biological barrier, that is

$$\beta_{ML} = \delta_o^{-1} D_{o,ML}/(a^{-1} D_{ML}) \tag{28}$$

After some algebra, the solutions x and y to eqs 26 and 27 can be written in the closed form expressions

$$\begin{cases} x = \dfrac{(\lambda + \beta_{ML})(1 - a_M^{-1}) + Bn_M^{-1}(1 + \gamma_{ML} + \beta_{ML}) + \gamma_M \beta_{ML}}{2a_M^{-1}[\lambda + (1 + \gamma_M)\beta_{ML}]} \left\{ -1 + \dfrac{|(\lambda + \beta_{ML})(1 - a_M^{-1}) + Bn_M^{-1}(1 + \gamma_{ML} + \beta_{ML}) + \gamma_M \beta_{ML}|}{(\lambda + \beta_{ML})(1 - a_M^{-1}) + Bn_M^{-1}(1 + \gamma_{ML} + \beta_{ML}) + \gamma_M \beta_{ML}} \times \right. \\ \left. \sqrt{1 + 4a_M^{-1} \dfrac{(\lambda + \beta_{ML})[\lambda + \beta_{ML}(1 + \gamma_M)]}{[(\lambda + \beta_{ML})(1 - a_M^{-1}) + Bn_M^{-1}(1 + \gamma_{ML} + \beta_{ML}) + \gamma_M \beta_{ML}]^2}} \right\} & \text{(a)} \\ y = \dfrac{1 + \gamma_{ML} x}{1 + \beta_{ML} + \gamma_{ML}} & \text{(b)} \end{cases} \tag{29}$$

where λ is defined by $\lambda = 1 + \gamma_M + \gamma_{ML}$. The normalized fluxes $Q_{i=M,ML} = J_{u,i}/J_{u,i}^{max}$ then directly follow upon substitution of x and y given by eq 29 into eq 6 (or eq 9) and eq 25. In the linear Henry regime for M bioaccumulation applicable for $a_M = K_{u,M}/c_M^{*} \gg 1$, it is straightforward to verify that the corresponding expressions of $Q_{i=M,ML} = J_{u,i}/J_{u,i}^{max}$ (x and y) are exactly those given by eqs 23 (eqs 21, respectively) after replacing therein the reciprocal ML Bosma number, Bn_{ML}^{-1}, by β_{ML}. In turn, under Henry bioaccumulation conditions, the biouptake scenarios in Figures 1B become formally equivalent, with the ML internalization conductance term $K_{H,ML}k_{int,ML}$ (m s^{-1}) in Figure 1B playing the role of the ML barrier diffusion conductance $D_{o,ML}\delta_o^{-1}$ (m s^{-1}) in Figure 1C.

3.3.2.3. Scenario Where M and ML Are Internalized by a Single Facilitated Diffusion Pathway (Figure 1D). 3.3.2.3.1. Competitive Inhibition. In this scenario schemed in Figures 1D and 2A, M and ML species are bioaccumulated via a shared facilitated diffusion pathway where they compete for the same type of *active* sites of the transport protein in the cell plasma membrane. In turn, the fluxes $J_{u,i=M,ML}$ are defined by Michaelis−Menten expressions corrected for such a M/ML competitive inhibition according to[37]

https://doi.org/10.1021/acsenvironau.5c00293
ACS Environ. Au XXXX, XXX, XXX−XXX

$$\begin{cases} J_{u,M}/J_{u,M}^{max} = x/[a_M(1 + y/a_{ML}) + x] & (a) \\ J_{u,ML}/J_{u,ML}^{max} = y/[a_{ML}(1 + x/a_M) + y] & (b) \end{cases} \quad (30)$$

Following the strategy adopted for the bioaccumulation scenarios considered previously, the M and ML surface concentrations x and y, respectively, are derived from the steady-state condition $J_{u,i=M,ML} = J_{i=M,ML}$ (eq 8), where $J_{i=M,ML}$ and $J_{u,i=M,ML}$ are given by eqs 6 and 30, respectively. After some algebra, we find that x and y are governed by the following new coupled quadratic equations

$$\begin{cases} A_2x^2 + A_1(y)x + A_0(y^2, y) = 0 & (a) \\ B_2y^2 + B_1(x)y + B_0(x^2, x) = 0 & (b) \end{cases} \quad (31)$$

where $A_0(y^2, y)$, $B_0(x^2, x)$, $A_1(y)$ and $B_1(x)$ are now functions of y^2, y, x^2, and/or x, and A_2 and B_2 are constants defined by

$$\begin{cases} \begin{bmatrix} A_0(y^2, y) \\ A_1(y) \\ A_2 \end{bmatrix} = & (a) \\ \quad \begin{bmatrix} -(1 + a_{ML}^{-1}y)(1 + \gamma_M y) \\ (1 + a_{ML}^{-1}y)(1 + \gamma_M) + Bn_M^{-1} - a_M^{-1}(1 + \gamma_M y) \\ a_M^{-1}(1 + \gamma_M) \end{bmatrix} \\ \begin{bmatrix} B_0(x^2, x) \\ B_1(x) \\ B_2 \end{bmatrix} = & (b) \\ \quad \begin{bmatrix} -(1 + a_M^{-1}x)(1 + \gamma_{ML} x) \\ (1 + a_M^{-1}x)(1 + \gamma_{ML}) + Bn_{ML}^{-1} - a_{ML}^{-1}(1 + \gamma_{ML} x) \\ a_{ML}^{-1}(1 + \gamma_{ML}) \end{bmatrix} \end{cases} \quad (32)$$

where the parameters $a_{M,ML}$, $\gamma_{M,ML}$ and $Bn_{M,ML}$ have all been defined in the preceding developments. Equations 31 and 32 can be solved numerically (Section 3.4), and the fluxes $J_{u,i=M,ML}$ are subsequently obtained by substituting the solutions found for x and y in eq 30 (or, equivalently, in eq 6). In the linear M and ML Henry bioaccumulation regimes reached for sufficiently low values of M and ML bioaffinities (i.e., $a_{i=M,ML} \gg 1$), eq 30 simplifies into the linearized expressions $J_{u,M} = K_{H,M}k_{int,M}c_M^{(a)}$ and $J_{u,ML} = K_{H,ML}k_{int,ML}c_{ML}^{(a)}$ which do not involve any term related to M/ML competitive inhibition. Accordingly, M/ML competitive inhibition becomes insignificant in the M and ML Henry bioaccumulation regimes, and the scenario in Figures 1D and 2A then becomes strictly and formally identical to the one sketched in Figure 1B (cf. Section 3.3.2.1). In turn, in the limits $a_{i=M,ML} \gg 1$, the defining expressions for the M and ML surface concentrations and for the normalized M and ML biouptake fluxes for the competitive inhibition scenario reduce to eqs 21 and 23, respectively.

3.3.2.3.2. Mixed Competitive Inhibition. In this situation illustrated by Figures 1D and 2D, M and ML are translocated across the biological barrier via a single facilitated diffusion pathway, and both species compete not only for the active sites of the transport protein but also for nonactive (inhibitory) sites. More specifically, while the binding of M and ML to the active transporter sites refers to the competitive inhibition case treated in the previous section, the mixed inhibition scenario also involves the binding of M and ML to the ML-transporter and M-transporter complexes, respectively, via inhibitory sites. Accordingly, in addition to the M and ML bioaffinity parameters $a_{i=M,ML} = K_{u,i}/c_i^*$, we introduce here the dimensionless M and ML bioaffinity parameters for the nonactive sites of the ML-transporter and M-transporter complexes, respectively, denoted as $a_{(I),i=M,ML} = K_i^{(I)}/c_{u,i}^*$. The constants $K_{i=M,ML}^{(I)}$ (in mol m^{-3}) correspond to the reciprocals of the stability constants describing the binding of M and ML with the nonactive (inhibitory) sites of the protein transporters. The biouptake fluxes $J_{u,i=M,ML}$ can be then written as a function of the surface concentrations x and y according to the following forms[37]

$$\begin{cases} J_{u,M}/J_{u,M}^{max} = x/[a_M(1 + y/a_{ML}) + x(1 + y/a_{(I),ML})] & (a) \\ J_{u,ML}/J_{u,ML}^{max} = y/[a_{ML}(1 + x/a_M) + y(1 + x/a_{(I),M})] & (b) \end{cases} \quad (33)$$

Application of the steady-state condition $J_{u,i=M,ML} = J_{i=M,ML}$ (eq 8) where $J_{i=M,ML}$ and $J_{u,i=M,ML}$ are given by eqs 6 and 33, respectively, leads to the following set of coupled polynomial equations in x and y

$$\begin{cases} A_2(y)x^2 + A_1(y^2, y)x + A_0(y^2, y) = 0 & (a) \\ B_2(x)y^2 + B_1(x^2, x)y + B_0(x^2, x) = 0 & (b) \end{cases} \quad (34)$$

where the functions $A_0(y^2, y)$, $B_0(x^2, x)$, $A_1(y^2, y)$ and $B_1(x^2, x)$, $A_2(y)$, and $B_2(x)$ are now defined by

https://doi.org/10.1021/acsenvironau.5c00293
ACS Environ. Au XXXX, XXX, XXX−XXX

$$\begin{cases} \begin{bmatrix} A_0(y^2, y) \\ A_1(y^2, y) \\ A_2(y) \end{bmatrix} \\ \quad = \begin{bmatrix} -(1 + a_{\mathrm{ML}}^{-1}y)(1 + \gamma_{\mathrm{M}}y) \\ (1 + a_{\mathrm{ML}}^{-1}y)(1 + \gamma_{\mathrm{M}}) + Bn_{\mathrm{M}}^{-1} \\ \quad - a_{\mathrm{M}}^{-1}(1 + \gamma_{\mathrm{M}}y)(1 + a_{(\mathrm{I}),\mathrm{ML}}^{-1}y) \\ a_{\mathrm{M}}^{-1}(1 + \gamma_{\mathrm{M}})(1 + a_{(\mathrm{I}),\mathrm{ML}}^{-1}y) \end{bmatrix} \quad \text{(a)} \\ \begin{bmatrix} B_0(x^2, x) \\ B_1(x^2, x) \\ B_2(x) \end{bmatrix} \\ \quad = \begin{bmatrix} -(1 + a_{\mathrm{M}}^{-1}x)(1 + \gamma_{\mathrm{ML}}x) \\ (1 + a_{\mathrm{M}}^{-1}x)(1 + \gamma_{\mathrm{ML}}) + Bn_{\mathrm{ML}}^{-1} - a_{\mathrm{ML}}^{-1}(1 \\ \quad + \gamma_{\mathrm{ML}}x)(1 + a_{(\mathrm{I}),\mathrm{M}}^{-1}x) \\ a_{\mathrm{ML}}^{-1}(1 + \gamma_{\mathrm{ML}})(1 + a_{(\mathrm{I}),\mathrm{M}}^{-1}x) \end{bmatrix} \quad \text{(b)} \end{cases} \tag{35}$$

Equations 34 and 35 must be solved numerically to obtain x and y and subsequently evaluate the M and ML uptake fluxes $Q_{i=\mathrm{M,ML}} = J_{\mathrm{u},i}/J_{\mathrm{u},i}^{\max}$ via use of eq 33 (or eq 6). In the limit where M and ML bioaffinities to the inhibitory sites are so low that $a_{(\mathrm{I}),i=\mathrm{M,ML}}^{-1} \to 0$, it is easily verified that eqs 33−35 for the mixed inhibition scenario correctly reduce to eqs 30−32 applicable to the competitive inhibition case. Lastly, in the extreme where $a_{(\mathrm{I}),i=\mathrm{M,ML}}^{-1} \to 0$ and $a_{i=\mathrm{M,ML}} \gg 1$, it is also straightforward to verify from eq 33 that the biouptake scenario considered here becomes formally similar to that where M and ML are internalized by different facilitated diffusion pathways within the linear Henry bioaccumulation regimes (Figure 1B, Section 3.3.2.1): expressions of x, y and $Q_{i=\mathrm{M,ML}} = J_{\mathrm{u},i}/J_{\mathrm{u},i}^{\max}$ then reduce to eqs 21 and 23 in these regimes, respectively.

3.3.2.3.3. Noncompetitive Inhibition. The noncompetitive inhibition situation (Figures 1D and 2B) may be viewed as a particular case of the mixed competitive inhibition scenario where M and ML bioaffinity parameters for the active and inhibitory sites are identical, i.e., $a_{(\mathrm{I}),i=\mathrm{M,ML}} = a_{i=\mathrm{M,ML}}$.[42] In this limit, eq 34 is still valid, and eqs 33 and 35 simplify into

$$\begin{cases} J_{\mathrm{u,M}}/J_{\mathrm{u,M}}^{\max} = x/[(x + a_{\mathrm{M}})(1 + y/a_{\mathrm{ML}})] & \text{(a)} \\ J_{\mathrm{u,ML}}/J_{\mathrm{u,ML}}^{\max} = y/[(y + a_{\mathrm{ML}})(1 + x/a_{\mathrm{M}})] & \text{(b)} \end{cases} \tag{36}$$

and

$$\begin{cases} \begin{bmatrix} A_0(y^2, y) \\ A_1(y^2, y) \\ A_2(y) \end{bmatrix} = \\ \quad \begin{bmatrix} -(1 + a_{\mathrm{ML}}^{-1}y)(1 + \gamma_{\mathrm{M}}y) \\ (1 + a_{\mathrm{ML}}^{-1}y)[1 + \gamma_{\mathrm{M}} - a_{\mathrm{M}}^{-1}(1 + \gamma_{\mathrm{M}}y)] + Bn_{\mathrm{M}}^{-1} \\ a_{\mathrm{M}}^{-1}(1 + \gamma_{\mathrm{M}})(1 + a_{\mathrm{ML}}^{-1}y) \end{bmatrix} \quad \text{(a)} \\ \begin{bmatrix} B_0(x^2, x) \\ B_1(x^2, x) \\ B_2(x) \end{bmatrix} = \\ \quad \begin{bmatrix} -(1 + a_{\mathrm{M}}^{-1}x)(1 + \gamma_{\mathrm{ML}}x) \\ (1 + a_{\mathrm{M}}^{-1}x)[1 + \gamma_{\mathrm{ML}} - a_{\mathrm{ML}}^{-1}(1 + \gamma_{\mathrm{ML}}x)] + Bn_{\mathrm{ML}}^{-1} \\ a_{\mathrm{ML}}^{-1}(1 + \gamma_{\mathrm{ML}})(1 + a_{\mathrm{M}}^{-1}x) \end{bmatrix} \quad \text{(b)} \end{cases} \tag{37}$$

respectively. The M and ML uptake fluxes $Q_{i=\mathrm{M,ML}} = J_{\mathrm{u},i}/J_{\mathrm{u},i}^{\max}$ are then obtained from eq 36 where x and y are solutions of eq 34 with $A_0(y^2, y)$, $B_0(x^2, x)$, $A_1(y^2, y)$, $B_1(x^2, x)$, $A_2(y)$, and $B_2(x)$ being defined by eq 37.

3.3.2.3.4. Uncompetitive Inhibition. The uncompetitive inhibition situation (Figures 1D and 2C) corresponds to a mixed competitive inhibition (eqs 33−35, Figures 1D and 2D) in the limit where M and ML bioaffinities for the nonactive inhibitory sites are much larger than those for their respective active sites, i.e., $a_{(\mathrm{I}),i=\mathrm{M,ML}}^{-1} \gg a_{\mathrm{i=M,ML}}^{-1}$.[42] In such a limit, it is straightforward to verify that eq 33 defining M and ML biouptake fluxes become

$$\begin{cases} J_{\mathrm{u,M}}/J_{\mathrm{u,M}}^{\max} = x/[a_{\mathrm{M}} + x(1 + y/a_{(\mathrm{I}),\mathrm{ML}})] & \text{(a)} \\ J_{\mathrm{u,ML}}/J_{\mathrm{u,ML}}^{\max} = y/[a_{\mathrm{ML}} + y(1 + x/a_{(\mathrm{I}),\mathrm{M}})] & \text{(b)} \end{cases} \tag{38}$$

and that the M and ML surface concentrations x and y are now determined by the coupled polynomial equations

$$\begin{cases} A_2(y)x^2 + A_1(y^2, y)x + A_0(y) = 0 & \text{(a)} \\ B_2(x)y^2 + B_1(x^2, x)y + B_0(x) = 0 & \text{(b)} \end{cases} \tag{39}$$

where the functions $A_0(y)$, $B_0(x)$, $A_1(y^2, y)$, $B_1(x^2, x)$, $A_2(y)$, and $B_2(x)$ are here provided by

https://doi.org/10.1021/acsenvironau.5c00293
ACS Environ. Au XXXX, XXX, XXX−XXX

Table 1. Theoretical Expressions Defining the Dimensionless M and ML Surface Concentrations (x and y, Respectively) and Dimensionless Biouptake Fluxes ($Q_{i=M,ML}$) for the Metal Bioaccumulation Scenarios Pictured in Figures 1 and 2 (Specified)[a]

M is the only bioreactive metal form (Figure 1A, case ❶)

Biouptake flux(es)	Expressions of x and y	Expressions of $Q_{i=M,ML}$
$\begin{cases} Q_M = J_{u,M}/J_{u,M}^{max} = x/(a_M + x) \\ Q_{ML} = J_{u,ML}/J_{u,ML}^{max} = 0 \end{cases}$	*Rigorous* $\begin{cases} x = \left(1 - a_M - b_M + (1 + a_M + b_M)\sqrt{1 - \frac{4b_M}{(1 + a_M + b_M)^2}}\right)/2 \\ y = (1 + \gamma_{ML}x)/(1 + \gamma_{ML}) \end{cases}$ *Approximate* (valid for $a_M = K_{u,M}/c_M^* \gg 1$) $x = 1/\left(1 + (pBn_M)^{-1}\right)\ ;\ y = 1 + \xi(x-1)$	*Rigorous* $\begin{cases} Q_M = \frac{1}{2}\left(\frac{1 + a_M + b_M}{b_M}\right)\left(1 - \sqrt{1 - \frac{4b_M}{(1 + a_M + b_M)^2}}\right) \\ Q_{ML} = 0 \end{cases}$ *Approximate* (valid for $a_M = K_{u,M}/c_M^* \gg 1$) $Q_M = a_M^{-1}/\left(1 + (pBn_M)^{-1}\right)$

M and ML are bioreactive metal forms

M and ML are internalized by different facilitated diffusion pathways (Figure 1B, case ❷)

Biouptake flux(es)	Expressions of x and y	Expressions of $Q_{i=M,ML}$
$\begin{cases} Q_M = J_{u,M}/J_{u,M}^{max} = x/(a_M + x) \\ Q_{ML} = J_{u,ML}/J_{u,ML}^{max} = y/(a_{ML} + y) \end{cases}$	*Rigorous* Defined by $\begin{cases} A_2x^2 + A_1(y)x + A_0(y) = 0 \\ B_2y^2 + B_1(x)y + B_0(x) = 0 \end{cases}$, where $\begin{cases} \begin{bmatrix} A_0(y) \\ A_1(y) \\ A_2 \end{bmatrix} = \begin{bmatrix} -(1+\gamma_M y) \\ 1 + \gamma_M + Bn_M^{-1} - a_M^{-1}(1+\gamma_M y) \\ a_M^{-1}(1+\gamma_M) \end{bmatrix} \\ \begin{bmatrix} B_0(x) \\ B_1(x) \\ B_2 \end{bmatrix} = \begin{bmatrix} -(1+\gamma_{ML}x) \\ 1 + \gamma_{ML} + Bn_{ML}^{-1} - a_{ML}^{-1}(1+\gamma_{ML}x) \\ a_{ML}^{-1}(1+\gamma_{ML}) \end{bmatrix} \end{cases}$ *Approximate* (valid for $a_{i=M,ML} = K_{u,i}/c_i^* \gg 1$) $\begin{cases} x = 1/\left\{1 + \frac{1 + \left[1 + (\eta Bn_M - 1)\xi\right]Bn_{ML}^{-1}}{1 + (1-\xi)(pBn_M)^{-1}}(pBn_M)^{-1}\right\} \\ y = \left[1 + \xi(x-1)\right]/\left[1 + (1-\xi)Bn_{ML}^{-1}\right] \end{cases}$	*Approximate* (valid for $a_{i=M,ML} = K_{u,i}/c_i^* \gg 1$) $\begin{cases} Q_M = a_M^{-1}Bn_M\left\{1 + \frac{(pBn_M)^{-1}\left[\eta\xi + (\xi - p)\psi\right] - 1}{1 + (pBn_M)^{-1}\left\{1 + \psi\left[(1-\xi)(1 + Bn_M^{-1}) + \eta\xi\right]\right\}}\right\} \\ Q_{ML} = a_{ML}^{-1}Bn_{ML}\left\{1 + \frac{(pBn_M)^{-1}(\xi\psi - 1) - 1}{1 + (pBn_M)^{-1}\left\{1 + \psi\left[(1-\xi)(1 + Bn_M^{-1}) + \eta\xi\right]\right\}}\right\} \end{cases}$

M and ML are internalized by facilitated and passive diffusions, respectively (Figure 1C, case ❸)

Biouptake flux(es)	Expressions of x and y
$\begin{cases} Q_M = J_{u,M}/J_{u,M}^{max} = x/(a_M + x) \\ J_{u,ML} = D_{o,ML}c_{ML}^*(y - y_o)/\delta_o \end{cases}$	*Rigorous* $\begin{cases} x = \frac{(\lambda + \beta_{ML})\left(1 - a_M^{-1}\right) + Bn_M^{-1}(1 + \gamma_{ML} + \beta_{ML}) + \gamma_M\beta_{ML}}{2a_M^{-1}\left[\lambda + (1+\gamma_M)\beta_{ML}\right]} \times \left\{-1 + \frac{\left|(\lambda + \beta_{ML})\left(1 - a_M^{-1}\right) + Bn_M^{-1}(1 + \gamma_{ML} + \beta_{ML}) + \gamma_M\beta_{ML}\right|}{(\lambda + \beta_{ML})\left(1 - a_M^{-1}\right) + Bn_M^{-1}(1 + \gamma_{ML} + \beta_{ML}) + \gamma_M\beta_{ML}} \times \right. \\ \left. \sqrt{1 + 4a_M^{-1}\frac{(\lambda + \beta_{ML})\left[\lambda + \beta_{ML}(1+\gamma_M)\right]}{\left[(\lambda + \beta_{ML})\left(1 - a_M^{-1}\right) + Bn_M^{-1}(1 + \gamma_{ML} + \beta_{ML}) + \gamma_M\beta_{ML}\right]^2}}\right\}\ ;\ y = \frac{1 + \gamma_{ML}x}{1 + \beta_{ML} + \gamma_{ML}} \end{cases}$ *Approximate* (valid for $a_{i=M,ML} = K_{u,i}/c_i^* \gg 1$) : as in ❷ after replacing Bn_{ML}^{-1} by β_{ML}
	Expressions of $Q_{i=M,ML}$
	Approximate (valid for $a_{i=M,ML} = K_{u,i}/c_i^* \gg 1$) : as in ❷ after replacing Bn_{ML}^{-1} by β_{ML}

M and ML are bioreactive metal forms

M and ML are internalized by a single facilitated diffusion pathway *with competitive inhibition* (Figures 1D-2A, ❹)

Biouptake flux(es)	Expressions of x and y	Expressions of $Q_{i=M,ML}$
$\begin{cases} Q_M = J_{u,M}/J_{u,M}^{max} = \frac{x}{a_M(1 + y/a_{ML}) + x} \\ Q_{ML} = J_{u,ML}/J_{u,ML}^{max} = \frac{y}{a_{ML}(1 + x/a_M) + y} \end{cases}$	*Rigorous* Defined by $\begin{cases} A_2x^2 + A_1(y)x + A_0(y^2, y) = 0 \\ B_2y^2 + B_1(x)y + B_0(x^2, x) = 0 \end{cases}$, where $\begin{cases} \begin{bmatrix} A_0(y^2,y) \\ A_1(y) \\ A_2 \end{bmatrix} = \begin{bmatrix} -\left(1 + a_{ML}^{-1}y\right)(1+\gamma_M y) \\ \left(1 + a_{ML}^{-1}y\right)(1+\gamma_M) + Bn_M^{-1} - a_M^{-1}(1+\gamma_M y) \\ a_M^{-1}(1+\gamma_M) \end{bmatrix} \\ \begin{bmatrix} B_0(x^2,x) \\ B_1(x) \\ B_2 \end{bmatrix} = \begin{bmatrix} -\left(1 + a_M^{-1}x\right)(1+\gamma_{ML}x) \\ \left(1 + a_M^{-1}x\right)(1+\gamma_{ML}) + Bn_{ML}^{-1} - a_{ML}^{-1}(1+\gamma_{ML}x) \\ a_{ML}^{-1}(1+\gamma_{ML}) \end{bmatrix} \end{cases}$ *Approximate* (valid for $a_{i=M,ML} = K_{u,i}/c_i^* \gg 1$): as in ❷	*Approximate* (valid for $a_{i=M,ML} = K_{u,i}/c_i^* \gg 1$) : as in ❷

M and ML are internalized by a single facilitated diffusion pathway *with mixed competitive inhibition* (Figures 1D-2D, ❺)

Biouptake flux(es)	Expressions of x and y	Expressions of $Q_{i=M,ML}$
$\begin{cases} Q_M = J_{u,M}/J_{u,M}^{max} = \frac{x}{a_M(1 + y/a_{ML}) + x(1 + y/a_{(I),ML})} \\ Q_{ML} = J_{u,ML}/J_{u,ML}^{max} = \frac{y}{a_{ML}(1 + x/a_M) + y(1 + x/a_{(I),M})} \end{cases}$	*Rigorous* Defined by $\begin{cases} A_2(y)x^2 + A_1(y^2, y)x + A_0(y^2, y) = 0 \\ B_2(x)y^2 + B_1(x^2, x)y + B_0(x^2, x) = 0 \end{cases}$, where $\begin{cases} \begin{bmatrix} A_0(y^2,y) \\ A_1(y^2,y) \\ A_2(y) \end{bmatrix} = \begin{bmatrix} -\left(1 + a_{ML}^{-1}y\right)(1+\gamma_M y) \\ \left(1 + a_{ML}^{-1}y\right)(1+\gamma_M) + Bn_M^{-1} - a_M^{-1}(1+\gamma_M y)\left(1 + a_{(I),ML}^{-1}y\right) \\ a_M^{-1}(1+\gamma_M)\left(1 + a_{(I),ML}^{-1}y\right) \end{bmatrix} \\ \begin{bmatrix} B_0(x^2,x) \\ B_1(x^2,x) \\ B_2(x) \end{bmatrix} = \begin{bmatrix} -\left(1 + a_M^{-1}x\right)(1+\gamma_{ML}x) \\ \left(1 + a_M^{-1}x\right)(1+\gamma_{ML}) + Bn_{ML}^{-1} - a_{ML}^{-1}(1+\gamma_{ML}x)\left(1 + a_{(I),M}^{-1}x\right) \\ a_{ML}^{-1}(1+\gamma_{ML})\left(1 + a_{(I),M}^{-1}x\right) \end{bmatrix} \end{cases}$ *Approximate* (valid for $a_{i=M,ML} = K_{u,i}/c_i^* \gg 1$ and $a_{(I),i=M,ML} = K_i^{(I)}/c_i^* \gg 1$) : as in ❷	*Approximate* (valid for $a_{i=M,ML} = K_{u,i}/c_i^* \gg 1$ and $a_{(I),i=M,ML} = K_i^{(I)}/c_i^* \gg 1$) : as in ❷

https://doi.org/10.1021/acsenvironau.5c00293
ACS Environ. Au XXXX, XXX, XXX−XXX

Table 1. continued

M and ML are bioreactive metal forms			
	M and ML are internalized by a single facilitated diffusion pathway *with non-competitive inhibition* (Figures 1D-2B, ❻)		
	Biouptake flux(es)	Expressions of x and y	Expressions of $Q_{i=M,ML}$
	$\begin{cases} Q_M = J_{u,M}/J_{u,M}^{max} = \dfrac{x}{(x+a_M)(1+y/a_{ML})} \\ Q_{ML} = J_{u,ML}/J_{u,ML}^{max} = \dfrac{y}{(y+a_{ML})(1+x/a_M)} \end{cases}$	*Rigorous* Defined by $\begin{cases} A_2(y)x^2 + A_1(y^2,y)x + A_0(y^2,y) = 0 \\ B_2(x)y^2 + B_1(x^2,x)y + B_0(x^2,x) = 0 \end{cases}$, where $\begin{cases} \begin{bmatrix} A_0(y^2,y) \\ A_1(y^2,y) \\ A_2(y) \end{bmatrix} = \begin{bmatrix} -(1+a_{ML}^{-1}y)(1+\gamma_M y) \\ (1+a_{ML}^{-1}y)[1+\gamma_M - a_M^{-1}(1+\gamma_M y)] + Bn_M^{-1} \\ a_M^{-1}(1+\gamma_M)(1+a_{ML}^{-1}y) \end{bmatrix} \\ \begin{bmatrix} B_0(x^2,x) \\ B_1(x^2,x) \\ B_2(x) \end{bmatrix} = \begin{bmatrix} -(1+a_M^{-1}x)(1+\gamma_{ML}x) \\ (1+a_M^{-1}x)[1+\gamma_{ML} - a_{ML}^{-1}(1+\gamma_{ML}x)] + Bn_{ML}^{-1} \\ a_{ML}^{-1}(1+\gamma_{ML})(1+a_M^{-1}x) \end{bmatrix} \end{cases}$ *Approximate* (valid for $a_{i=M,ML} = K_{u,i}/c_i^* \gg 1$) : as in ❷	*Approximate* (valid for $a_{i=M,ML} = K_{u,i}/c_i^* \gg 1$) : as in ❷
	M and ML are internalized by a single facilitated diffusion pathway *with uncompetitive inhibition* (Figures 1D-2C, ❼)		
	Biouptake flux(es)	Expressions of x and y	Expressions of $Q_{i=M,ML}$
	$\begin{cases} Q_M = J_{u,M}/J_{u,M}^{max} = x/\left[a_M + x\left(1+y/a_{(I),ML}\right)\right] \\ Q_{ML} = J_{u,ML}/J_{u,ML}^{max} = y/\left[a_{ML} + y\left(1+x/a_{(I),M}\right)\right] \end{cases}$	*Rigorous* Defined by $\begin{cases} A_2(y)x^2 + A_1(y^2,y)x + A_0(y) = 0 \\ B_2(x)y^2 + B_1(x^2,x)y + B_0(x) = 0 \end{cases}$, where $\begin{cases} \begin{bmatrix} A_0(y) \\ A_1(y^2,y) \\ A_2(y) \end{bmatrix} = \begin{bmatrix} -(1+\gamma_M y) \\ 1+\gamma_M + Bn_M^{-1} - a_M^{-1}(1+\gamma_M y)(1+a_{(I),ML}^{-1}y) \\ a_M^{-1}(1+\gamma_M)(1+a_{(I),ML}^{-1}y) \end{bmatrix} \\ \begin{bmatrix} B_0(x) \\ B_1(x^2,x) \\ B_2(x) \end{bmatrix} = \begin{bmatrix} -(1+\gamma_{ML}x) \\ 1+\gamma_{ML} + Bn_{ML}^{-1} - a_{ML}^{-1}(1+\gamma_{ML}x)(1+a_{(I),M}^{-1}x) \\ a_{ML}^{-1}(1+\gamma_{ML})(1+a_{(I),M}^{-1}x) \end{bmatrix} \end{cases}$ *Approximate* (valid for $a_{(I),i=M,ML} = K_i^{(I)}/c_i^* \gg 1$)) : as in ❷	*Approximate* (valid for $a_{(I),i=M,ML} = K_i^{(I)}/c_i^* \gg 1$)) : as in ❷

[a]The derivations of the results collated in this table are detailed in Section 3 and the limits reached within the linear Henry bioaccumulation regimes ($a_{i=M,ML} \gg 1$) and in the extreme where M/ML binding to inhibitory sites is insignificant ($a_{(I),i=M,ML} \gg 1$) are further specified.

$$\begin{cases} \begin{bmatrix} A_0(y) \\ A_1(y^2, y) \\ A_2(y) \end{bmatrix} = \\ \quad \begin{bmatrix} -(1+\gamma_M y) \\ 1+\gamma_M + Bn_M^{-1} - a_M^{-1}(1+\gamma_M y)(1+a_{(I),ML}^{-1}y) \\ a_M^{-1}(1+\gamma_M)(1+a_{(I),ML}^{-1}y) \end{bmatrix} \quad \text{(a)} \\ \begin{bmatrix} B_0(x) \\ B_1(x^2, x) \\ B_2(x) \end{bmatrix} = \\ \quad \begin{bmatrix} -(1+\gamma_{ML}x) \\ 1+\gamma_{ML} + Bn_{ML}^{-1} - a_{ML}^{-1}(1+\gamma_{ML}x)(1+a_{(I),M}^{-1}x) \\ a_{ML}^{-1}(1+\gamma_{ML})(1+a_{(I),M}^{-1}x) \end{bmatrix} \quad \text{(b)} \end{cases} \tag{40}$$

Within the framework of the bioaccumulation scenario considered here, the dimensionless M and ML uptake fluxes $Q_{i=M,ML} = J_{u,i}/J_{u,i}^{max}$ are thus obtained from eq 38 where x and y are solutions of eq 39 and the functions $A_0(y)$, $B_0(x)$, $A_1(y^2, y)$, $B_1(x^2, x)$, $A_2(y)$, and $B_2(x)$ are defined by eq 40.

3.4. Summary, Validation of the Numerical and Analytical Surface Concentration and Flux Computations

As a summary, Table 1 reports the expressions we derived for the M and ML surface concentrations, x and y, and the normalized M and ML biouptake fluxes, $Q_{i=M,ML} = J_{u,i}/J_{u,i}^{max}$, applicable to each metal bioaccumulation scenario shown in Figures 1 and 2. In all cases, evaluating these fluxes requires solving a set of two polynomial equations in x and y that involve the quantities $A_{0,1,2}$ and $B_{0,1,2}$ we defined earlier for each bioaccumulation situation. Closed-form solutions for x, y, and $Q_{i=M,ML}$ can be rigorously obtained only for the bioaccumulation scenarios depicted in Figure 1A,C. For all other cases, explicit approximate solutions are obtainable under the Henry bioaccumulation conditions, where $Q_{i=M,ML}$ depend linearly on x and y. For all situations addressed in the Results and Discussion section, the numerical evaluation of x and y at fixed values of the model parameters specifying M/ML speciation, diffusion and biouptake (cf. details in Section 4), was performed by solving the relevant set of coupled polynomial equations within the Mathcad Prime 8.0 calculus environment and use of the Levenberg−Marquardt solving algorithm. The M and ML biouptake fluxes were then computed by substituting the obtained x and y values into the relevant expressions of $Q_{i=M,ML}$. We systematically verified that the numerical outcomes properly compared to predictions from rigorous or approximate analytical solutions within the range of applicable values of model parameters. Finally, we stress that the validity of all analytical developments detailed in Section 3 was systematically verified using the symbolic calculus capabilities of Mathcad Prime 8.0. All codes are available upon request.

4. RESULTS AND DISCUSSION

We present and discuss here illustrative numerical simulations that detail the dependence of metal bioaccumulation fluxes $Q_{i=M,ML}$ on the relevant biophysiochemical parameters

https://doi.org/10.1021/acsenvironau.5c00293
ACS Environ. Au XXXX, XXX, XXX−XXX

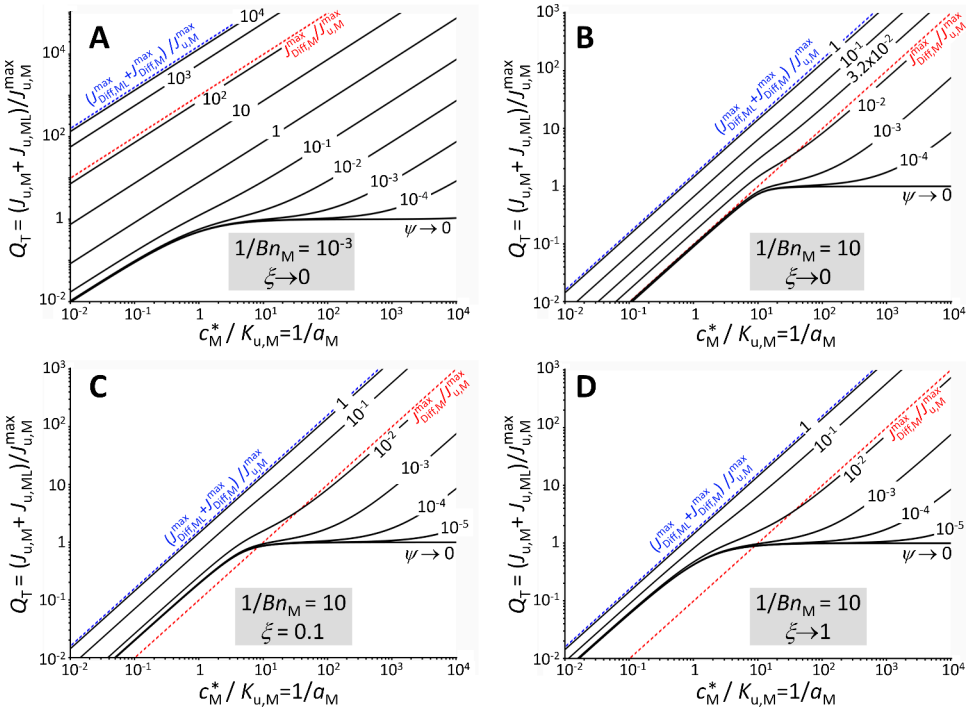

Figure 5. Dependence of the (dimensionless) total metal biouptake flux Q_T (eq 41) on the normalized free metal concentration for the situation where free M and the ML complex are internalized via distinct facilitated diffusion pathways (eqs 9, 17−20, Figure 1B). The normalization factor is the reciprocal M affinity constant for the M-internalization sites, $K_{u,M}$. The resulting ratio $c^*_M/K_{u,M}$ identifies with the reciprocal of the M bioaffinity parameter, $1/a_M$. Results are further given for various values of the reciprocal M and ML Bosma numbers, Bn_M^{-1} and Bn_{ML}^{-1} or, equivalently, Bn_M^{-1} and $\psi = (Bn_{ML}/Bn_M)^{-1}$ (eq 24), as specified. (A) M biouptake is rate-limited by the internalization step. (B−D) M biouptake is rate-limited by diffusion, and ML is (B) inert, (C) nonlabile, and (D) fully labile. Model parameters other than those provided in the figure: $1/a_{ML} = 1$, $\eta = 15$. The red and blue dotted lines represent the maximum diffusion flux of free M and the maximum diffusion flux of free M plus ML complex, respectively, both normalized by $J^{max}_{u,M}$.

involved in the theory developed in Section 3. Specifically, these parameters describe: (i) the interplay between metal speciation and diffusive transport ($\overline{K}_{ML}$, ξ, η), i.e., the chemodynamics and lability of ML complex, (ii) the bioaffinities of M and ML to the internalization and inhibitory sites ($a^{-1}_{i=M,ML}$, $a^{-1}_{(I),i=M,ML}$), and (iii) the kinetics of M/ML bioaccumulation, as subsumed in the Bosma numbers $Bn_{i=M,ML}$ and their ratio $\psi = (Bn_{ML}/Bn_M)^{-1}$. It is verified that specification of this set of dimensionless parameters (i)-(iii) is sufficient to fully describe the biouptake scenarios considered in Section 3 and schematically presented in Figures 1 and 2. Given that experimental reports classically represent metal bioaccumulation data as a function of free metal concentration, we provide below the evolution of the metal biouptake flux as a function of the dimensionless free metal concentration in the form of $c^*_M/K_{u,M}$, which is the reciprocal of the metal bioaffinity parameter $1/a_M$. Furthermore, unless e.g., specific isotopic labels are employed, it is virtually impossible to differentiate between internalized free and complexed metal forms from bioaccumulation experiments. Accordingly, we report below the normalized *total* metal biouptake flux, Q_T, defined by

$$\begin{aligned} Q_T &= (J_{u,M} + J_{u,ML})/J^{max}_{u,M} \\ &= Q_M + \eta(b_{ML}/b_M)Q_{ML} \\ &= Q_M + \eta\psi(a_{ML}/a_M)Q_{ML} \end{aligned} \quad (41)$$

where the second and third equalities are established using eq 24 and the expressions $Q_{i=M,ML} = J_{u,i}/J^{max}_{u,i}$, $\eta = \varepsilon\overline{K}_{ML}$, and $b_{i=M,ML} = J^{max}_{u,i}/(pJ^{max}_{Diff,i})$ (cf. Sections 3.1 and 3.2).

4.1. Illustrative Computational Results

4.1.1. Bioaccumulation Scenario Where M and ML Are Each Internalized by Their Own Distinct Facilitated Diffusion Pathway and There Is No Competition (Figure 1B). Figure 5 shows the total metal biouptake flux, Q_T, as a function of M affinity for the active sites ($1/a_M$) for various Bosma number ratios, $\psi = (Bn_{ML}/Bn_M)^{-1}$. As detailed in the theory section, for $\psi \to 0$ (bold black curve featuring the plateau value at $1/a_M \gg 1$), the intact ML complex is not taken up and Q_T corresponds solely to $J_{u,M}$ (which includes any M dissociated from ML as determined by the degree of ML lability, ξ). For $\psi \to 0$, the plateau in Q_T obtained at large values of $1/a_M$ corresponds to saturation of the active biouptake sites for M, at which point the normalized flux approaches unity (as prescribed by the Michaelis−Menten equation). At the other extreme, for sufficiently large values of ψ, uptake of ML is diffusion-limited ($1/Bn_{ML} \gg 1$) and Q_T then approaches the maximum diffusive flux for ML, $J^{max}_{Diff,ML}$ (blue dashed lines) under the conditions of Figure 5 where $\eta \gg 1$. Figure 5A−D illustrates the interplay between M bioaccumulation kinetics, subsumed in its Bosma number (Bn_M), and the lability of ML (quantified by ξ). In Figure 5A, ML is inert ($\xi \to 0$) and thus ML does not contribute to M

https://doi.org/10.1021/acsenvironau.5c00293
ACS Environ. Au XXXX, XXX, XXX−XXX

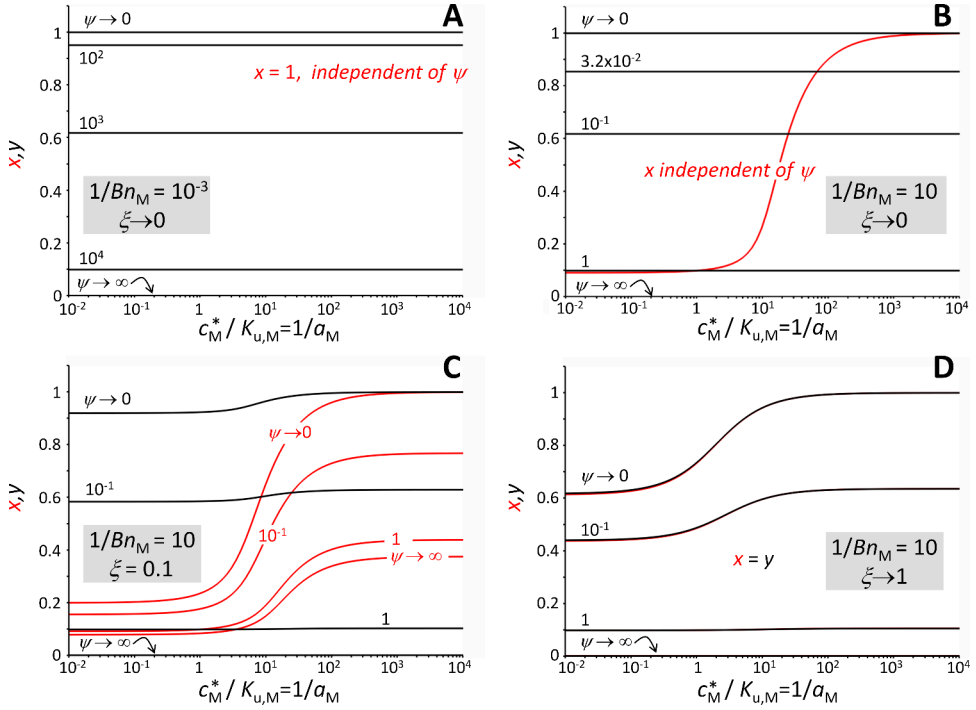

Figure 6. Dependence of the (dimensionless) M and ML surface concentrations $x = c_M^{(a)}/c_M^*$ (red) and $y = c_{ML}^{(a)}/c_{ML}^*$ (black), respectively, on the normalized free metal concentration $c_M^*/K_{u,M} = 1/a_M$ (which is the reciprocal of the M bioaffinity parameter) for the situation where free M and the ML complex are internalized via distinct facilitated diffusion pathways (eqs 9, 17−20, Figure 1B). Results are presented under the conditions of Figure 5 for various values of the reciprocal M and ML Bosma numbers, Bn_M^{-1} and Bn_{ML}^{-1} or, equivalently, Bn_M^{-1} and $\psi = (Bn_{ML}/Bn_M)^{-1}$ (eq 24), as specified. (A) M biouptake is rate-limited by the internalization step. (B−D) M biouptake is rate-limited by diffusion, and ML is (B) inert, (C) nonlabile, and (D) fully labile. Model parameters other than those provided in the figure: as in Figure 5. In (D), the red and black curves (x and y, respectively) are superimposed.

biouptake (and vice versa). In addition, we have $Bn_M^{-1} \ll 1$, thus there is no diffusion limitation for M biouptake, i.e., the internalization step is rate-limiting and there is no concentration gradient in M at the biointerface ($x = c_M^{(a)}/c_M^* = 1$, independent of ψ, red line in Figure 6A). Accordingly, when ML is not taken up ($\psi \to 0$), Q_T remains well below the diffusive flux limit for M, $J_{Diff,M}^{max}$ (red dashed line in Figure 5A). As ψ increases, at a given $1/a_M$ the contribution to Q_T from uptake of ML increases until the diffusive limit for ML is attained (blue dashed line in Figure 5A). At high values of $1/a_M$, the increase in Q_T above the saturation plateau with increasing ψ corresponds solely to only ML uptake. The surface concentration of ML $\left(y = c_{ML}^{(a)}/c_{ML}^*\right)$ evolves accordingly: as ψ increases, the uptake of ML increases and the surface concentration of ML decreases and ultimately approaches zero for $\psi \to \infty$ (black lines in Figure 6A).

In Figure 5B, ML is still inert ($\xi \to 0$) and thus does not contribute to M biouptake. Also, we have $Bn_M^{-1} = 10$, thus M biouptake is now limited by M diffusion from the bulk solution and a concentration gradient in M develops at the biointerface ($x = c_M^{(a)}/c_M^*$ is independent of ψ due to inert ML, cf. red line in Figure 6B). Accordingly, when ML is not taken up ($\psi \to 0$), Q_T corresponds here to the maximum diffusive flux for M, $J_{Diff,M}^{max}$ (red dashed line) until saturation of the active sites is reached (at sufficiently high $1/a_M$) (Figure 5B). In the Henry regime, the surface concentration of M is $x \approx Bn_M$ (Figure 3), it then increases as $1/a_M$ increases, eventually reaching a plateau of unity corresponding to saturation of the active M sites, at which point internalization has become rate-limiting (Figure 6B). The evolutions of Q_T and $y = c_{ML}^{(a)}/c_{ML}^*$ as a function of ψ (Figure 5B and 6B) follow the same trend as described for Figures 5A and 6A.

In Figure 5C, ML is nonlabile ($\xi = 0.1$) and thus dissociation kinetics determine the extent to which ML can contribute to M biouptake, and $Bn_M^{-1} = 10$, thus M biouptake is diffusion-limited by M diffusion from the bulk solution. Now, when ML is not taken up ($\psi \to 0$), so long as the M active sites are not saturated (i.e., in the Henry regime at sufficiently low $1/a_M$), Q_T exceeds the maximum diffusive flux for M, $J_{Diff,M}^{max}$ (red dashed line), which reflects the contribution from M dissociated from ML. Since ML is nonlabile, there is some degree of coupling between the surface concentrations of M and ML (Figure 6C). For example, when $\psi \to 0$ there is no uptake of ML, but as the bioaffinity for M increases (i.e., as $1/a_M$ increases), the surface concentration of M increases (red lines in Figure 6C) and thus so does the surface concentration of ML (black lines in Figure 6C). For these conditions ($Bn_M^{-1} \gg 1$, nonlabile ML), in the Henry regime, the ψ dependence of x is described by $x \approx [1 + \sqrt{\bar{\kappa}_a} Bn_{ML}]Bn_M$ when $Bn_{ML}^{-1} \gg 1$ (Figure 3). At the other extreme, when there is diffusion-limited uptake of ML ($\psi \to \infty$) and the surface concentration of ML approaches zero, the plateau in the surface concentration of M at large $1/a_M$ is less than unity

https://doi.org/10.1021/acsenvironau.5c00293
ACS Environ. Au XXXX, XXX, XXX−XXX

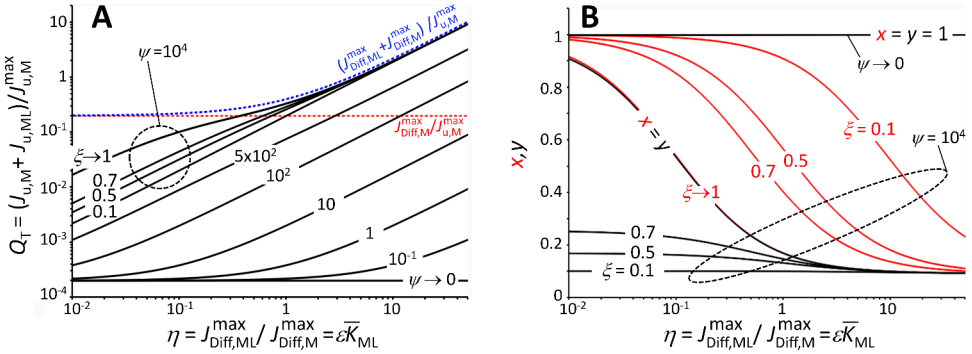

Figure 7. Dependence of the (dimensionless) (A) total metal biouptake flux Q_T (eq 41) and (B) M/ML surface concentrations $x = c_M^{(a)}/c_M^*$ (red) and $y = c_{ML}^{(a)}/c_{ML}^*$ (black), on the ratio $\eta = J_{Diff,ML}^{max}/J_{Diff,M}^{max} = \varepsilon\bar{K}_{ML}$. The considered situation is that where free M and ML complex are internalized via distinct facilitated diffusion pathways (eqs 9, 17−24, Figure 1B). Results are presented for $Bn_M^{-1} = 10^{-3}$ and various values of $\psi = (Bn_{ML}/Bn_M)^{-1}$ (eq 24), as specified. For the specific case $\psi = 10^4$, i.e., $Bn_{ML}^{-1} = 10$, results are given for various values of the ML lability, ξ, as specified. For situations where $Bn_{M,ML}^{-1} \ll 1$, results do not depend on ξ (i.e., ML is inert). Model parameters other than those provided in the figure: $1/a_M = 2 \times 10^{-4}$, $1/a_{ML} = 0.1$. See text for details. In (A), the red and blue dotted lines represent the maximum diffusion flux of free M and the maximum diffusion flux of free M plus ML complex, respectively, both normalized by $J_{u,M}^{max}$.

because the local equilibrium is shifted toward the formation of ML (Figure 6C).

In Figure 5D, ML is now labile ($\xi \to 1$) and thus fully contributes to M biouptake via coupled M-ML diffusion, and the condition $Bn_M^{-1} = 10$ is here maintained so that M biouptake is still diffusion-limited. As compared to the nonlabile case (Figure 5C), below saturation of the M active sites, Q_T for $\psi \to 0$ (no ML uptake) exhibits greater exceedance of the maximum diffusive flux for M, $J_{Diff,M}^{max}$ (red dashed line) which is a consequence of the complete buffering of the M concentration by labile ML at all spatial scales. This is reflected in the surface concentration profiles for M and ML which are now fully coupled in accordance with the lability of the system (Figures 3 and 6D). At sufficiently large $1/a_M$ when saturation of M active sites is achieved, the M and ML concentration gradients disappear, i.e., internalization has become rate limiting. Surface depletion of M at low $1/a_M$ in the presence of labile ML (Figure 6D) is less than that for nonlabile ML (Figure 6C) because M is fully buffered by the dissociation of ML. As ψ increases, the contribution of ML increases and as $\psi \to \infty$, ML uptake is dominant (independent of $1/a_M$) and the surface concentrations of both M and ML approach zero.

Further insights are obtained by considering the dependence of Q_T and the surface concentrations of M and ML on the ratio $\eta = J_{Diff,ML}^{max}/J_{Diff,M}^{max} = \varepsilon\bar{K}_{ML}$ at various degrees of ML lability (Figure 7). As ψ increases, the contribution of ML increases, and Q_T becomes increasingly sensitive to ML lability, ξ, as highlighted in Figure 7A for $\psi = 10^4$. In this ψ-regime, as ξ increases, M is increasingly able to buffer the surface concentration of ML and thus Q_T increases and the surface concentrations of M and ML evolve accordingly (Figure 7B, and also Figures 6C,D). At sufficiently large values of η and ψ, the total flux Q_T becomes predominantly limited solely by ML diffusion from bulk solution (blue dashed line in Figure 7A), it becomes accordingly independent of ML lability and it well exceeds the maximum flux of M diffusion from solution (red dashed line). Interestingly, unlike common practice in the BLM literature, Figure 7A shows that metal complex (ML) lability can be a determining biouptake factor even when the metal internalization flux is well below the maximum metal diffusion supply flux. This is because the ML complex itself can be taken up—a hypothesis that the BLM framework rejects from the outset and which is rarely validated or justified *a posteriori*.

4.1.2. Bioaccumulation Scenario Where M and ML Are Internalized Via a Single Shared Facilitated Diffusion Pathway. *4.1.2.1. M and ML Competitive Inhibition.* In this case, the biouptake fluxes $J_{u,M}$ and $J_{u,ML}$ are defined by the Michaelis−Menten expressions corrected for competitive inhibition, eq 30. Making the analogy with first-principles of enzymatic kinetic theory, M and ML competitive inhibition results in an apparent increase of the M and ML half-saturation constants, $K_{u,M}$ and $K_{u,ML}$ (or, equivalently, $a_{M,ML}$) while leaving unaffected the maximum uptake fluxes, $J_{u,M}^{max}$ and $J_{u,ML}^{max}$, respectively.[37,42] Figure 8 presents the total (dimensionless) uptake flux, Q_T, the ML uptake flux, Q_{ML}, and the surface concentrations of M and ML as a function of the reciprocal of M bioaffinity parameter for the active sites ($1/a_M$), and for various values of the ML bioaffinity parameter, a_{ML}. Figure 8A−C shows the results for the case of inert ML ($\xi = 0$), and no diffusion limitation of M uptake ($Bn_M^{-1} \ll 1$). At $\psi \to 0$ there is no uptake of ML and Q_T thus corresponds solely to M uptake (black dashed line, Figure 8A). As a_{ML} increases at fixed value of ψ (solid black curves, Figure 8A), the competitive effect of ML on M uptake decreases and thus, at a given $1/a_M$, Q_T increases with increasing a_{ML} and attains a maximal plateau value at lower $1/a_M$, i.e., less M affinity is needed to overcome ML competition (Figure 8A). Consistent with these effects, as a_{ML} increases (i.e., decreasing ML affinity for the internalization sites), Q_{ML} decreases and approaches zero at progressively higher $1/a_M$ due to the decreasing ability of ML to compete with M uptake (Figure 8B). In the given example, both Bn_M^{-1} and Bn_{ML}^{-1} are ≪1, thus there is no

https://doi.org/10.1021/acsenvironau.5c00293
ACS Environ. Au XXXX, XXX, XXX−XXX

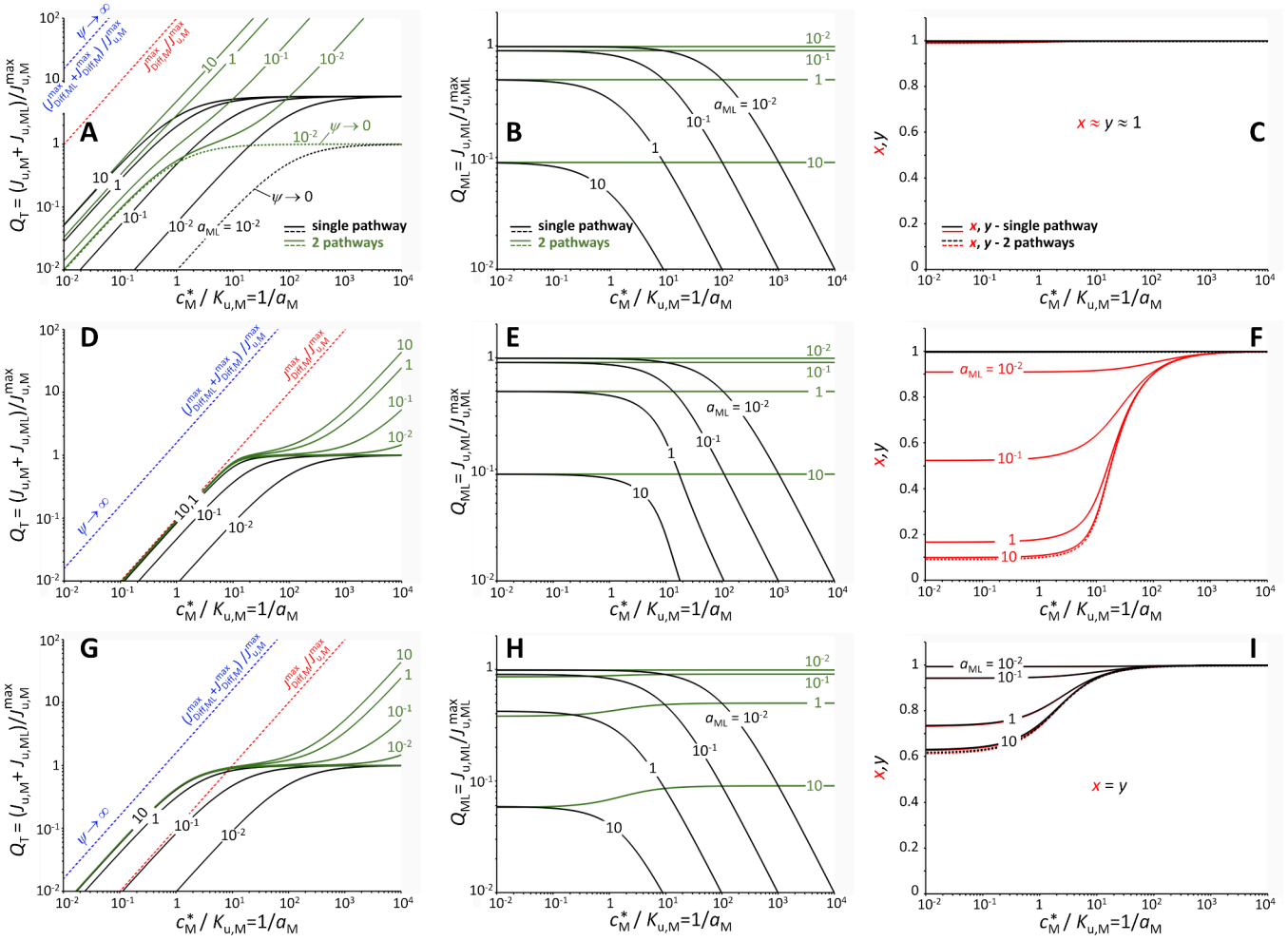

Figure 8. Dependence of the (dimensionless) (A, D, G) total metal biouptake flux Q_T (eq 41); (B,E,H) corresponding ML biouptake flux Q_{ML} and (C, F, I) associated M/ML surface concentrations $x = c_M^{(a)}/c_M^*$ (red) and $y = c_{ML}^{(a)}/c_{ML}^*$ (black), on the normalized free metal concentration $c_M^*/K_{u,M} = 1/a_M$, for the situation where free M and ML complex are internalized via a single facilitated diffusion pathway with *competitive* inhibition (eqs 30−32, Figures 1D and 2A). Results are presented for various values of the ML bioaffinity parameter a_{ML} (specified), with (A−C) $Bn_M^{-1} = 10^{-2}$ and $\xi = 0$; (D−F) $Bn_M^{-1} = 10$ and $\xi = 0$; and (G, H, I) $Bn_M^{-1} = 10$ and $\xi \to 1$. In each panel, the computations pertaining to the limit where there is no competitive inhibition (eqs 9, 17−20, Figure 1B) are indicated in green color (A, B, D, E, G, H) and in dotted lines (C, F, I), as specified. This limit formally corresponds to the one where M and ML biouptake proceeds according to 2 distinct pathways. In (A), the dotted black and green lines are predictions for $\psi \to 0$ or, equivalently, $Bn_{ML}^{-1} \to 0$. These predictions coincide in (D, G) with results given for $a_{ML} = 10^{-2}$. In (A, D, G), the red and blue dotted lines represent the maximum diffusion flux of free M and the maximum diffusion flux of free M plus ML complex, respectively, both normalized by $J_{u,M}^{max}$. In (C, F, I), x and y do not depend on a_{ML} in the limit of 2 bioaccumulation pathways. Model parameters other than those provided in the figure: $\eta = 15$ and $Bn_{ML}^{-1} = 10^{-2.5}$.

diffusion limitation of M or ML and no concentration gradient at the biointerface, i.e., $x \approx y = 1$ (Figure 8C). At large $1/a_M$, Q_{ML} then reaches a limiting value equal to $\sim 1/(a_{ML}/a_M)$ (eq 30) and the resulting total uptake flux $Q_T = Q_M + \eta\psi(a_{ML}/a_M)Q_{ML}$ (cf. eq 41) then reduces to $Q_T = Q_M + \eta\psi$. For the conditions selected in Figure 8A, we have $\eta = 15$ and $\psi = 0.316$ (solid black curves), which yields $Q_T = 5.74$ at large $1/a_M$.

Figure 8D−F reports the results for the case of inert ML ($\xi = 0$) and diffusion limitation of M uptake ($Bn_M^{-1} = 10$). Figure 8D shows that when ML competition is low (i.e., $a_{ML} \geq 1$), Q_T corresponds to the maximum diffusive flux of M, $J_{Diff,M}^{max}$ (below saturation of the active sites, black curves coincident with the red dashed line). As ML competition increases (decreasing a_{ML}) at a given $1/a_M$ value, Q_T decreases. As compared to Figure 8B, Q_{ML} is here basically greater at a given a_{ML} due to the diffusion limitation of M uptake (Figure 8E). This is a consequence of the lower surface concentration of M (Figure 8F), and thus the more effective competition by ML. As ML competition increases (i.e., as a_{ML} decreases), the surface concentration of M increases (Figure 8F) and M uptake becomes less impacted by the diffusion limitation. The limiting value of Q_T at large $1/a_M$ is close to unity ($\eta = 15$ and $\psi = 3.16 \times 10^{-4}$). Since $Bn_{ML}^{-1} \ll 1$, there is no diffusion limitation of ML and thus no concentration gradient at the biointerface ($y = 1$, Figure 8F).

Figure 8G−I details the results for the case of labile ML ($\xi \to 1$) and diffusion limitation of M uptake ($Bn_M^{-1} = 10$).

https://doi.org/10.1021/acsenvironau.5c00293
ACS Environ. Au XXXX, XXX, XXX−XXX

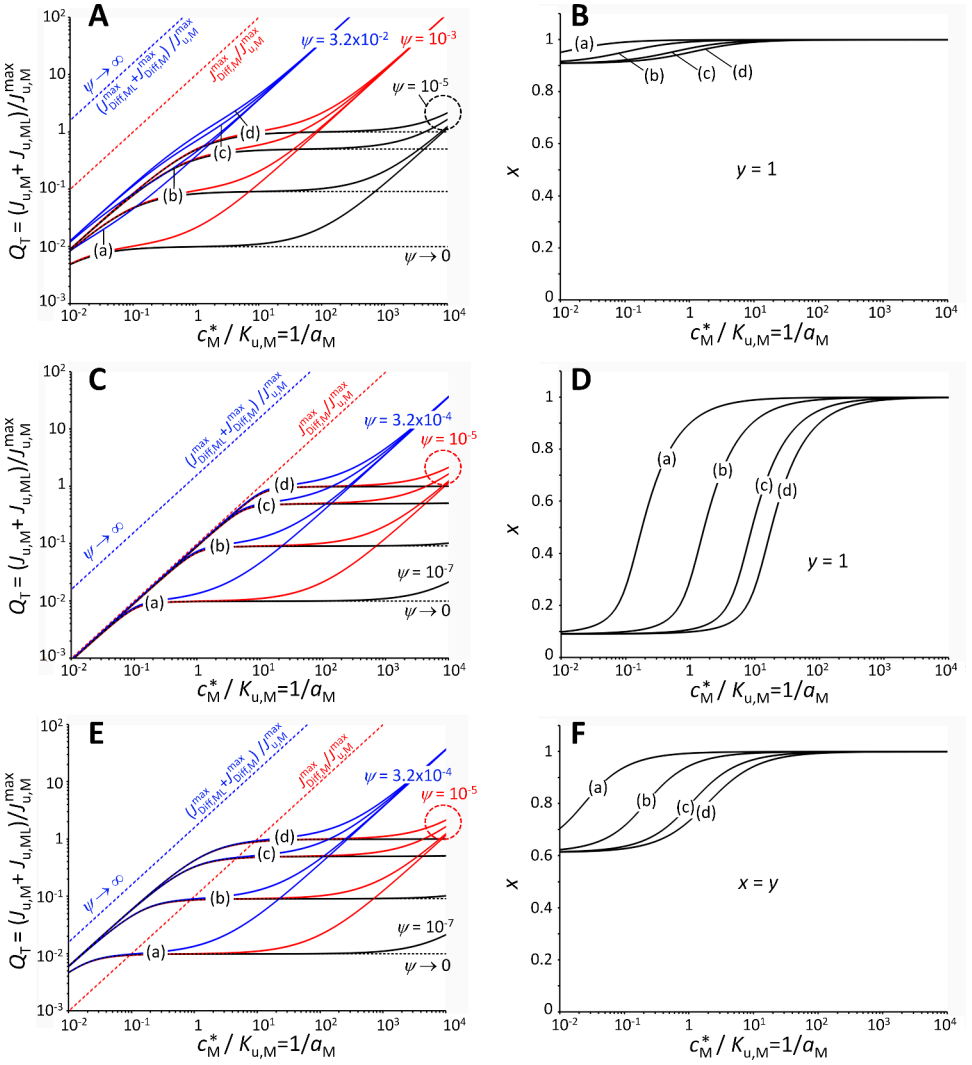

Figure 9. Dependence of the (dimensionless) (A, C, E) total metal biouptake flux Q_T (eq 41) and (B, D, F) corresponding M/ML surface concentrations $x = c_M^{(a)}/c_M^*$ and $y = c_{ML}^{(a)}/c_{ML}^*$, on the normalized free metal concentration $c_M^*/K_{u,M} = 1/a_M$, for the situation where free M and ML complex are internalized via a single facilitated diffusion pathway with *uncompetitive* inhibition (eqs 38−40, Figures 1D and 2C). Results are presented for various values of the ML bioaffinity parameter $a_{(I),ML}$, with $a_{(I),ML} = 10^{-2}$ (a), 10^{-1} (b), 1 (c), 10^3 (d), for (A, B) $Bn_M^{-1} = 10^{-1}$ and $\xi = 0$; (C, D) $Bn_M^{-1} = 10$ and $\xi = 0$; (E, F) $Bn_M^{-1} = 10$ and $\xi \to 1$. In each panel, the computations are further provided for $\psi \to 0$ (black dotted lines) and three other specified values of ψ (black, red, and blue solid lines). In (A, C, E), the red and blue dotted lines represent the maximum diffusion flux of free M and the maximum diffusion flux of free M plus ML complex, respectively, both normalized by $J_{u,M}^{max}$. In (B, D, F), x and y do not depend on ψ. Model parameters other than those provided in the figure: $1/a_{(I),M} \to 0$, $1/a_{ML} = 0.3$, $\eta = 15$. Under the conditions examined in (A, B) and (C, D), we have $Q_{ML} \approx 0.23$ regardless of $a_{(I),ML}$ and ψ. Under the conditions examined in (E, F), the variations of Q_{ML} with changing $a_{(I),ML}$ are shown in Figure S1, SI−C.

The general trends are the same as the preceding case except that now when ML competition is low ($a_{ML} \geq 1$), Q_T exceeds the maximum diffusive flux of M, due to buffering of the M concentration by labile ML (Figure 8G). As ML competition increases (i.e., as a_{ML} decreases), Q_T decreases here again at a given $1/a_M$ value, i.e., progressively greater M bioaffinity is needed to overcome the increasing ML competition. As $\psi \to \infty$, Q_T approaches the diffusion limit for ML, $J_{Diff,ML}^{max}$ (blue dashed line). The evolution of Q_{ML} as a function of a_{ML} and a_M lies intermediate between those presented in Figure 8B,E, and it reflects the coupled surface concentration profiles of M and ML (Figure 8I), i.e., ML lability inherently results in mutual buffering of M and ML at all spatial scales, thereby moderating the effect of ML competition as compared to the inert case (for which there is no concentration gradient in ML; Figure 8F).

In the absence of competitive inhibition (green lines in Figure 8), the situation becomes formally similar to that when ML and M are taken up by 2 uncoupled internalization pathways (Section 3, Figures 5−7). Under such conditions, there is no plateau in Q_T at large $1/a_M$ (Figure 8A,D,G) because Q_{ML} is constant (Figure 8B,E) or, in the case of labile ML, increases as $1/a_M$ increases (Figure 8H). In the latter case, the increase in Q_{ML} is due to buffering of the ML surface concentration by labile ML.

4.1.2.2. M and ML Uncompetitive Inhibition. In this case, the biouptake fluxes $J_{u,M}$ and $J_{u,ML}$ are defined by the Michaelis−Menten expressions corrected for uncompetitive

https://doi.org/10.1021/acsenvironau.5c00293
ACS Environ. Au XXXX, XXX, XXX−XXX

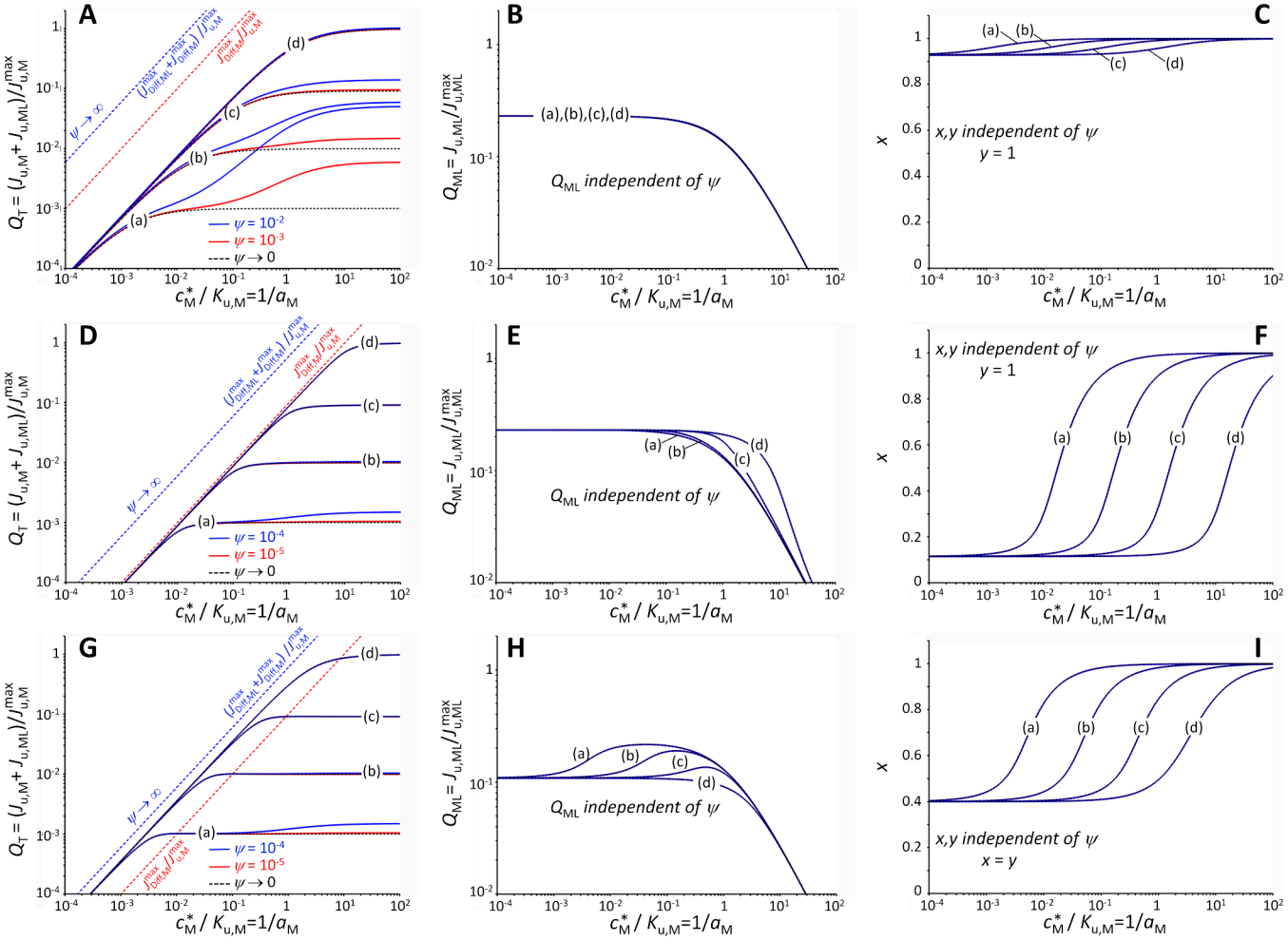

Figure 10. Dependence of the (dimensionless) (A, D, G) total metal biouptake flux Q_T (eq 41); (B, E, H) corresponding ML biouptake flux Q_{ML} and (C, F, I) associated M/ML surface concentrations $x = c_M^{(a)}/c_M^*$ and $y = c_{ML}^{(a)}/c_{ML}^*$, on the normalized free metal concentration $c_M^*/K_{u,M} = 1/a_M$, for the situation where free M and ML complex are internalized via a single facilitated diffusion pathway with *mixed competitive* inhibition (eqs 33−35, Figures 1D and 2D). Results are presented for various values of the ML bioaffinity parameter $a_{(I),ML}$, with $a_{(I),ML} = 10^{-3}$ (a), 10^{-2} (b), 10^{-1} (c), 10^{2} (d), for (A−C) $Bn_M^{-1} = 10^{-1}$ and $\xi = 0$; (D−F) $Bn_M^{-1} = 10$ and $\xi = 0$; (G−I) $Bn_M^{-1} = 10$ and $\xi \to 1$. In each panel, the computations are further provided for $\psi \to 0$ (black dotted lines) and two other specified values of ψ (blue and red solid lines). In (A, D, G), the red and blue dotted lines represent the maximum diffusion flux of free M and the maximum diffusion flux of free M plus ML complex, respectively, both normalized by $J_{u,M}^{max}$. In (B, E, H) and (C, F, I), the quantities Q_{ML}, x, and y do not depend on ψ. Model parameters other than those provided in the figure: $1/a_{(I),M} \to 0$, $1/a_{ML} = 0.3$, $\eta = 5$. The noncompetitive inhibition limit reached for $a_{ML} = a_{(I),ML}$ is intermediate between cases (c) and (d) under the here examined conditions.

inhibition, eq 38. Under such conditions, drawing the analogy with enzyme kinetic theory,[37,42] uncompetitive inhibition results in an apparent and similar decrease in both $K_{u,M}$ and $J_{u,M}^{max}$. We consider below the internalization of M and ML via a single shared facilitated diffusion pathway including uncompetitive inhibition of ML on M uptake. That is, for illustrative purposes, it is assumed that M has no uncompetitive effect on ML uptake and thus Q_{ML} is given by the standard expression, eq 9 (i.e., $1/a_{(I),M} \to 0$ in eq 38). Figure 9 presents the total uptake flux, Q_T, and the surface concentrations of M and ML as a function of the affinity of M for the active sites ($1/a_M$), for various values of the ML bioaffinity parameter for the nonactive inhibitory sites, $a_{(I),ML}$ (and with considering a fixed ML bioaffinity parameter for the active sites, a_{ML}). At $\psi \to 0$, there is no ML contribution to the uptake and the plateau in Q_T at large $1/a_M$ corresponds to saturation of the M internalization sites (with accounting for the inhibitory effect of ML). As $a_{(I),ML}$ increases, the inhibitory effect of ML on M uptake decreases, and thus the Q_T plateau increases and approaches unity, as illustrated by the black dashed curves (a) → (d) in Figure 9A,C,E. As ψ increases, the contribution of ML increases, as evidenced by the increases in Q_T beyond the plateau at sufficiently large $1/a_M$. When ML is inert and uptake of M is diffusion-limited (Figure 9C), the point at which Q_T increases beyond the plateau is shifted to greater $1/a_M$ as compared to the nondiffusion-limited case (Figure 9A). This result is a consequence of the lower surface concentration of M in the diffusion-limited case (Figure 9D) and thus the more effective is uncompetitive inhibition by ML at a given bulk M concentration. When ML is labile, and uptake of M is diffusion-limited (Figure 9E), the lability of ML buffers the M and ML surface concentrations (Figure 9F) and thus moderates the impact of the uncompetitive inhibition. As

https://doi.org/10.1021/acsenvironau.5c00293
ACS Environ. Au XXXX, XXX, XXX−XXX

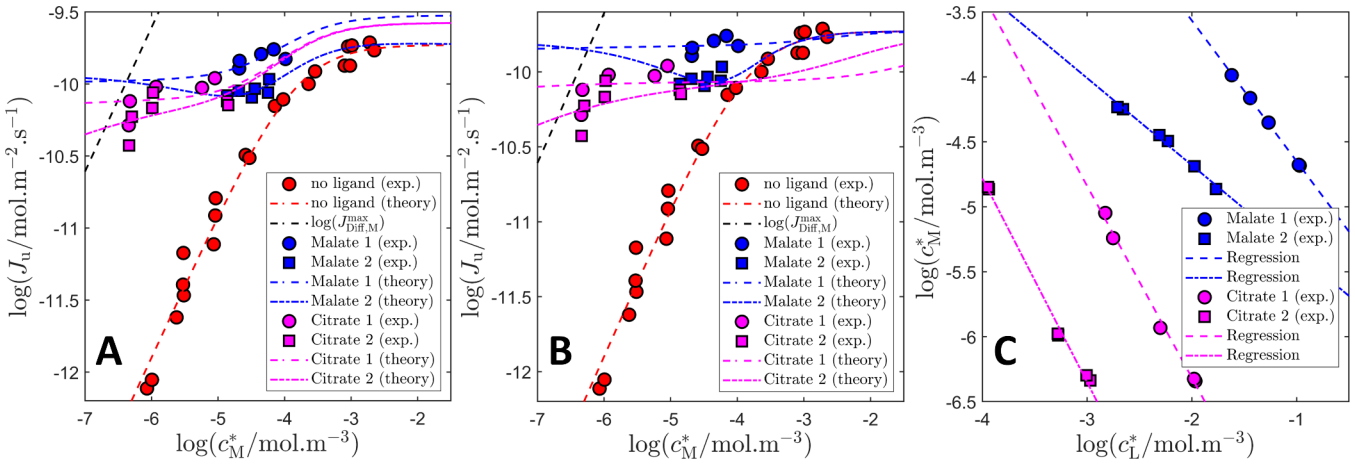

Figure 11. (A, B) Measured Nd (=M) bioaccumulation flux, J_u, by *Chlamydomonas reinhardtii* (symbols) as a function of the free Nd concentration, $c^*_{M=Nd}$ (log−log representation). Experiments were conducted in the presence and absence of the ligand (L), specifically malic acid or citric acid (as specified in the legend boxes). Measurements were quantitatively interpreted using theory, represented by dashed and dotted lines (cf. legend boxes). For cases where a ligand was present, theoretical fitting of the measured data was attempted by considering two scenarios: (A) two separate and uncoupled bioaccumulation pathways for Nd and Nd-L complexes (eqs 9, 17−20) and (B) a single, shared bioaccumulation pathway with competitive inhibition (eqs 30−32). (C) The combinations of concentrations of the ligand and free Nd concentrations used in the experiments are specified by the symbols, while dotted and dashed lines refer to log−log regressions of these data. The model parameters obtained from fitting the data to theory are compiled in Table 2. The maximum diffusion flux of M (dashed black lines in (A) and (B)) is given by $J^{max}_{Diff,M} = D_M c^*_M/a$, where D_M is corrected for the diffusion layer thickness in moderately stirred solution, as detailed in the caption of Table 2. See main text for details.

detailed for the preceding cases, Q_T in the Henry regime (low $1/a_M$) lies below $J^{max}_{Diff,M}$ when M uptake is not diffusion-limited (Figure 9A), is equal to $J^{max}_{Diff,M}$ when M uptake is diffusion-limited and ML is inert (Figure 9C), and exceeds $J^{max}_{Diff,M}$ when M uptake is diffusion-limited and ML is labile (and approaches $J^{max}_{Diff,ML}$ as $\psi \to \infty$; Figure 9E).

4.1.2.3. M and ML Mixed Competitive Inhibition, and the Noncompetitive Inhibition Limit. For illustrative purposes herein, we assume that ML acts as a mixed competitive inhibitor for the uptake of M (eq 33), and that M affects the uptake of ML via only competitive inhibition, i.e., $1/a_{(I),M} \to 0$ in eq 33. We further recall that the noncompetitive case (eq 36) refers to a limit of the mixed competitive situation (eq 33) where the affinity of e.g., ML for the active and nonactive uptake sites is the same, i.e., $a_{(I),ML} = a_{ML}$. Figure 10 presents the total uptake flux, Q_T, the ML uptake flux, Q_{ML}, and the surface concentrations of M and ML as a function of the affinity of M for the active sites ($1/a_M$) and for various values of the affinity of ML for the nonactive inhibitory sites, $a_{(I),ML}$. Under the conditions selected in Figure 10, the ML activity for the active sites, a_{ML}, is fixed, and the quantities Q_{ML}, x, and y are all independent of ψ essentially because $\psi \ll 1$.

Figure 10A−C shows the results for the case of inert ML, and no diffusion limitation of M uptake. Figure 10A shows that at $\psi \to 0$ (black dashed curve) there is no uptake of ML, and Q_T thus corresponds solely to M uptake. Under these conditions ($\psi \to 0$), the magnitude of the plateau in Q_T at large $1/a_M$ increases toward unity as the uncompetitive inhibition by ML decreases (curves (a) → (d), referring to increasing values of $a_{(I),ML}$). As ψ increases, the contribution from ML to the overall metal uptake increases and thus at large $1/a_M$, Q_T becomes greater than the plateau level attained for $\psi \to 0$. As discussed for the competitive competition case (Figure 8), at large $1/a_M$, Q_{ML} reaches a limiting value equal to $y/(a_{ML}/a_M)$ (Figure 10B), where y approaches unity at sufficiently high $1/a_M$ (Figure 10C). Thus, at large $1/a_M$, Q_{ML} approaches $1/(a_{ML}/a_M)$, and $Q_T = Q_M + \eta\psi$, cf. eq 41. For the conditions in Figure 10A, $\eta = 5$ and $\psi = 10^{-3}$ or 10^{-2}, which yields $Q_T = Q_M + 5 \times 10^{-3}$ (red curves) or $Q_M + 5 \times 10^{-2}$ (blue curves), respectively, at large $1/a_M$. In this example, Bn^{-1}_{ML} is rather low (being 10^{-3} for $\psi = 10^{-2}$ and 10^{-4} for $\psi = 10^{-3}$), thus the contribution from ML becomes negligible relative to that from M as the uncompetitive component of the ML mixed inhibition process decreases (curves (a) → (d)). As $1/a_{(I),ML} \to 0$ (curve (d)), this ML uncompetitive component becomes negligible, and the curves for all ψ values converge to that for $\psi \to 0$ (Figure 10A).

A similar trend in Q_T is observed when M uptake is diffusion-limited and ML is inert (Figure 10D). Due to the low ψ values used, the plateau in Q_T is practically the same as that for M only, and the contribution from ML is only evident at the greatest level of uncompetitive inhibition shown (curve (a)) ($\eta\psi$ is 5×10^{-4} or 5×10^{-5}, in blue and red curves, respectively). In the Henry regime (low $1/a_M$) Q_T is equal to $J^{max}_{Diff,M}$ and the curves are shifted to greater $1/a_M$ as compared to the nondiffusion-limited case (Figure 10A) due to the concentration gradient in M (Figure 10F), i.e., ML can compete more effectively at lower $1/a_M$. This finding is reflected in the evolution of the concentration gradient of M: as the uncompetitive component of the ML mixed inhibition decreases (curves (a) → (d)), the concentration gradient in M shifts to greater $1/a_M$ (Figure 10F). The trend in Q_{ML} (Figure 10E) reflects the coupling between the dependence of Q_{ML} on

https://doi.org/10.1021/acsenvironau.5c00293
ACS Environ. Au XXXX, XXX, XXX−XXX

Table 2. Fitted and Derived Parameters from the Analysis of Nd Bioaccumulation Data as a Function of Free Nd Concentration in the Absence or Presence of the Ligand (Malic Acid or Citric Acid) for *Chlamydomonas reinhardtii* (Log-log Representation, Figure 11)[27,a]

	Michaelis-Menten (MM) bioaccumulation					
M = Nd in the absence of ligand	$\log\left(J_{u,M}^{max}/\text{mol.m}^{2}.\text{s}^{-1}\right)$		$\log\left(K_{u,M}/\text{mol.m}^{-3}\right)$		Evaluated Bn_{M}^{-1}	
	-9.73 [-9.82 ; -9.64]		-3.83 [-3.96 ; -3.71]		7.44×10^{-3}	
	$R^2 = 0.98$					
Nd in the presence of ligand	**Distinct Michaelis-Menten biouptake pathways for Nd and Nd-L without competition**			**Single shared Michaelis-Menten biouptake pathway for Nd and Nd-L with competitive inhibition**		
	$\log\left(J_{u,ML}^{max}/\text{mol.m}^{2}.\text{s}^{-1}\right)$	$\log\left(K_{u,ML}/\text{mol.m}^{-3}\right)$	Derived $Bn_{M,ML}^{-1}$ and ψ	$\log\left(J_{u,ML}^{max}/\text{mol.m}^{2}.\text{s}^{-1}\right)$	$\log\left(K_{u,ML}/\text{mol.m}^{-3}\right)$	Derived $Bn_{M,ML}^{-1}$ and ψ
Nd and L = malic acid	-9.93 [-10.01 ; -9.85] $J_{u,ML}^{max}/J_{u,M}^{max} = 0.63$	-4.19 [-4.41 ; -3.97] $K_{u,ML}/K_{u,M} = 0.44$	$Bn_{ML}^{-1} = 1.06\times10^{-2}$ $\psi = 1.43$	-9.79 [-9.86 ; -9.73] $J_{u,ML}^{max}/J_{u,M}^{max} = 0.86$	-4.19 [-4.41 ; -3.96] $K_{u,ML}/K_{u,M} = 0.44$	$Bn_{ML}^{-1} = 1.45\times10^{-2}$ $\psi = 1.94$
	$R^2 = 0.87$			$R^2 = 0.85$		
Nd and L = citric acid	-10.10 [-10.24 ; -9.97] $J_{u,ML}^{max}/J_{u,M}^{max} = 0.42$	-4.00 [-4.73 ; -3.27] $K_{u,ML}/K_{u,M} = 0.68$	$Bn_{ML}^{-1} = 4.60\times10^{-3}$ $\psi = 0.62$	-10.06 [-10.19 ; -9.94] $J_{u,ML}^{max}/J_{u,M}^{max} = 0.46$	-3.91 [-4.53 ; -3.28] $K_{u,ML}/K_{u,M} = 0.85$	$Bn_{ML}^{-1} = 4.05\times10^{-3}$ $\psi = 0.54$
	$R^2 = 0.32$			$R^2 = 0.30$		

[a]Data analysis was performed according to metal bioaccumulation flux expressions relevant for the scenarios where Nd and Nd-L complexes are internalized via (i) two separate, uncoupled bioaccumulation pathways (eqs 9, 17−20, left column) or (ii) a single, shared bioaccumulation pathway with competitive inhibition (eqs 30−32, right column). Nd bioaccumulation data in the absence of the ligand were fitted according to eq 30 in the limits $J_{u,ML} \to 0$ and $1/a_{ML} \to 0$. Values in brackets correspond to the lower and upper bounds of the 95% confidence intervals. Other model parameters required for the fitting of data to theory were $a = 3.5\mu$m (cell radius);[27] $K_{ML} = 10^{2.52}$ m^3 mol^{-1} (Nd-malate) and $K_{ML} = 10^{5.7}$ m^3 mol^{-1} (Nd-citrate) being the stability constants applicable at the experimental ionic strength of 10 mM;[52] $D_{M,ML} = D_{M,ML}^{(0)}(a + \delta)/\delta$ (apparent diffusion coefficient including correction for gentle hydrodynamic stirring conditions) with $\delta = 8\ \mu$m[27,38,43−45] and $D_M^{(0)} \approx D_{ML}^{(0)} = 6 \times 10^{-10}$m^2 s^{-1} at 25 °C (diffusion coefficient uncorrected for convection).[53] The diffusion supply fluxes of M and ML are proportional to $D_{M,ML}/a$, i.e., $D_{M,ML}^{(0)}(a^{-1} + \delta^{-1})$, which correctly compares with the diffusion conductance term for moderately stirred solution.[38,43−45]

x/a_M ($y = 1$) and the dependence of x on $a_{(I),ML}$ (Figure 10F).

For the case where M uptake is diffusion-limited and ML is labile (Figure 10G), Q_T in the Henry regime (low $1/a_M$) exceeds $J_{Diff,M}^{max}$ due to the contribution from labile ML to the M flux. Again, the contribution from ML is barely discernible due to the low $\eta\psi$ values considered. The position of the Q_T curves on the $1/a_M$ axis is intermediate between those in Figure 10A,D because there are now concentration gradients in both M and ML (Figure 10I). Accordingly, the trend in Q_{ML} (Figure 10H) now reflects the intricate coupling between the dependence of Q_{ML} on x/a_M and y, together with the dependence of x on $a_{(I),ML}$ (Figure 10I).

5. APPLICATION TO THE INTERPRETATION OF MEASURED METAL BIOACCUMULATION DATA

The literature data from Yang et al.[27] selected for confrontation with theory (cf. Section 2) refer to the bioaccumulation of neodymium (M = Nd) by the unicellular green algae *Chlamydomonas reinhardtii* in the absence or presence of organic ligands (namely, L = malic acid or citric acid), Figure 11 (symbols), as a function of free Nd concentration. This specific data set was selected because it offers a very high level of experimental detail and consistency, which is essential for a rigorous confrontation with our theory. Critically, the original authors of this study demonstrated that the traditional Biotic Ligand Model (BLM) is not applicable for this system, as they observed an increase in metal biouptake flux with increasing ligand concentration. This makes the data set an ideal benchmark to test our framework, which specifically aims to elucidate "non-BLM" bioaccumulation scenarios where metal chemodynamics play a pivotal role. Furthermore, the data set provides experimental metal biouptake fluxes, effectively integrating the time dimension. These features—combined with well-characterized physicochemical medium composition and a broad range of tested metal concentrations in the presence and absence of well-defined organic ligands—provide the robust input parameters required to validate the interplay between metal chemodynamics and metal biouptake kinetics detailed by our theoretical framework. We sought to interpret these data sets by means of theory according to the two following different bioaccumulation scenarios: (i) Nd and Nd-L are internalized by two distinct facilitated diffusion pathways without competition (Figure 11A, eqs 9, 17−20), and (ii) Nd and Nd-L are internalized by a single facilitated diffusion pathway and there is competitive inhibition (Figure 11B, eqs 30−32). For both scenarios, we attempted to fit the data (in log−log format) using the relevant theoretical equations by iteratively adjusting the involved bioaffinity and maximum uptake flux

https://doi.org/10.1021/acsenvironau.5c00293
ACS Environ. Au XXXX, XXX, XXX−XXX

parameters, $K_{u,i=M,ML}$ and $J^{max}_{u,i=M,ML}$, respectively. The required values of $K_{u,M}$ and $J^{max}_{u,M}$ were obtained by first fitting the bioaccumulation data measured without ligand (i.e., by considering eq 30 in the limits $J_{u,ML} \to 0$ and $1/a_{ML} \to 0$). These values were then fixed when fitting the bioaccumulation data collected in the presence of L. Each data point referring in Figure 11A,B to measurement with a ligand corresponds to specific log−log combinations of concentrations of ligand and free Nd concentrations, which are detailed in Figure 11C (denoted as 'Malate 1,2' and 'Citrate 1,2'). Derivation of the model parameters for each envisaged bioaccumulation scenario was performed by fitting the two relevant data sets 1 and 2 concurrently. Theoretical predictions were then evaluated with adopting the so-obtained model parameters and by varying free and complexed Nd concentrations according to the log−log regressions shown in Figure 11C (dashed blue and pink lines in Figure 11A,B). Data analysis was performed using a custom MATLAB code that we developed for that purpose, which is available upon request. The results are summarized in Table 2, along with the adopted literature values for the diffusion coefficients of Nd and Nd-L, $D_{M,ML}$, for moderately stirred solution,[38,43−45] and the Nd-L complexation constants, K_{ML} (cf. caption Table 2). Data analysis leads to the following conclusions:

- the experimental data sets are fully consistent with the two types of bioaccumulation scenarios considered, as a similar goodness-of-fit is achieved for both cases (cf. R^2 values in Table 2);
- in both situations, diffusion-limited uptake of M and ML can be excluded. This is supported by our evaluation of the reciprocal Bosma numbers, $Bn^{-1}_{M,ML}$, which are both much lower than unity (cf. Table 2), and it is further confirmed by the independence of the theoretical fitting on the lability ξ of the Nd-L complex (which is inert);
- We note that the R^2 values for the citrate system are lower than those obtained for the malate system. This discrepancy is primarily due to the significantly higher experimental data scattering observed in the citrate data set, rather than a limitation of the theoretical framework itself. Specifically, a close inspection of the citrate data reveals that measurements taken at nearly identical free metal ion concentrations (representing experiments performed at different citric acid concentrations)—differing by only 0.01−0.02 log units in concentration (where concentration is in mol m^{-3})—exhibit biouptake fluxes (in mol m^{-2} s^{-1}) that differ by as much as 0.2 log units (cf. Figure 11A,B). Such intrinsic experimental variance necessarily limits the maximum achievable R^2 during the fitting process. Despite this scattering, the theory successfully captures the overall kinetic trends and the "nonstandard BLM" behavior of the system.

Yang et al.[27] interpreted their data sets by proposing that Nd and Nd-L bioaccumulation takes place via a shared diffusion facilitated pathway. However, our rigorous theoretical analysis demonstrates that it is impossible to distinguish between this scenario and one where Nd and Nd-L are taken up by two distinct, uncoupled pathways, particularly within the linear Henry biouptake regime. In this regime, theoretical expressions of the total metal flux are indeed identical for both models, as discussed in Section "Competitive Inhibition". A clear distinction between these two bioaccumulation scenarios can only be made if data are measured at free metal concentrations high enough to saturate the active M-sites (cf. Figure 11A vs Figure 11B). In the existing literature, a single, shared biouptake pathway is often invoked to interpret bioaccumulation data on metals, particularly trivalent ions such as rare earth metals and Al(III),[27,32,46−48] when the standard BLM model fails due to its nonaccount of ML bioavailability. Beyond the nonuniqueness of this interpretation, authors often exclude potential diffusion limitation (and ML lability contribution) by comparing $J_{u,M}$ with $J^{max}_{Diff,M}$ and arguing $J_{u,M}/J^{max}_{Diff,M} \ll 1$.[49−51] This reasoning, however, holds strictly only for the case where the intact ML complex is *not* bioaccumulated. If ML is taken up, diffusion limitation may be operational depending on the magnitude of the specific Bosma number that is operative for the very ML biouptake process. Furthermore, in scenarios where M and ML are thought to share a single uptake pathway, maximum M and ML uptake fluxes, $J^{max}_{u,i=M,ML}$, are commonly assumed to be identical.[27,32,46] We show here that while this approximation is practically valid for Nd and Nd-Malate complexes $\left(J^{max}_{u,ML}/J^{max}_{u,M} = 0.86\right)$, it is not for Nd and Nd-Citrate $\left(J^{max}_{u,ML}/J^{max}_{u,M} = 0.46\right)$, cf. Table 2. Ultimately, this work illustrates the significant benefits of using a mechanism-based Best-Michaelis−Menten formalism to interpret bioaccumulation data, moving beyond the common application of simple competitive adsorption isotherms.

In view of the above elements, the developed framework identifies and resolves several fundamental limitations of existing models by replacing empirical assumptions with a rigorous biophysical derivation. Most notably, the theory provides a formal mechanism to address the failure of the standard Biotic Ligand Model (BLM) in "nonstandard BLM" scenarios—specifically those where biouptake flux increases despite an increasing ligand concentration in solution. By rigorously excluding the often-unjustified assumption of complex inertness (via evaluation of the required Bosma numbers) and by quantifying the specific contribution of each bioreactive (internalizable) metal form (free and complexed) via derivation here of the parameter ψ, the theory offers a precise accounting of the overall metal biouptake. Furthermore, in case of citric acid data sets the derivation demonstrates the inadequacy of the common approximation done in the literature which consists of equating the maximum uptake fluxes for each bioreactive metal form, proving instead that these parameters are different for Nd metal and Nd-citrate complexes. Perhaps most significantly, the theory provides a mathematical justification for the fact that it is fundamentally impossible to discriminate between a single common uptake pathway and two distinct pathways for free and complexed metals based on bioaccumulation data collected within the Henry regime, as is the case for the herein analyzed data sets. This finding directly nuances conclusions currently found in the literature based on basic Michaelis−Menten arguments.

In turn, the framework developed herein addresses a long-standing gap in the literature regarding the connections between metal chemodynamics and biouptake kinetics of free metal and/or complexed metal species.[2] While the current validation focuses on neodymium due to the paucity of data sets providing a sufficiently broad range of metal concentrations and well-defined ligands, the resulting theoretical insights—such as the mathematical indistinguishability of

https://doi.org/10.1021/acsenvironau.5c00293
ACS Environ. Au XXXX, XXX, XXX−XXX

uptake pathways in the Henry metal bioaccumulation regime—possess a universal character. This approach is intended to serve as a foundational tool for interpreting non-BLM scenarios, including systems such as silver-thiosulfate which share mechanistic features with the Nd-malate/citrate systems discussed here.[31] Furthermore, this theory is intended to guide the design of future experiments, providing the necessary analytical framework to extract previously inaccessible information regarding the complex interplay between chemical speciation, bioavailability, and bioaccumulation.

6. CONCLUSIONS

This study presents a comprehensive theoretical framework to advance the understanding of kinetics of metal accumulation by aquatic organisms. Our model explicitly accounts for the dynamic interplay between metal speciation in the aquatic medium and the kinetics of biological uptake, thereby challenging the prevalent, equilibrium-based assumptions of the Biotic Ligand Model (BLM). This framework is particularly required in cases where the BLM fails, such as under high-metal complexation conditions, when the rate of metal biouptake is limited by metal diffusion from the bulk solution to the biosurface, or when metal complexes are bioreactive (i.e., internalizable) and/or feature some degree of lability. Our framework integrates the reactive transport of free and complexed metals within the biouptake scenarios identified in the literature as exceptions to the standard BLM.[2] These scenarios include the biouptake of lipophilic complexes, the internalization of free and complexed metals via distinct diffusion-facilitated uptake routes, or the formation of ternary metal−ligand complexes with active internalization sites shared by free and complexed metal species. By combining Michaelis−Menten biouptake kinetics, metal diffusion from the bulk solution and metal complexation kinetics in solution, we derive extended Best bioaccumulation flux expressions. These expressions define how the metal internalization flux depends on the relevant metal bioaffinity and complexation constants, as well as on the diffusion- and internalization-defining properties of both free metal ions and complexes. These expressions further account for the competitive, noncompetitive or uncompetitive inhibition operating between free and complexed metals when they share the same active sites on a membrane translocation protein. For all the biouptake cases considered, analytical expressions are elaborated where possible, especially for metal concentrations that align with the linear Henry bioaccumulation regime.

A detailed analysis of computated examples, which cover the biouptake situations mentioned previously, shows that a low metal uptake flux -relative to the maximum diffusion supply flux from solution- is not enough to conclude that only free metal is taken up and that ML lability is irrelevant. Instead, we demonstrate how the lability of metal complexes can be impacting the overall metal uptake flux, which depends on whether the complex itself is taken up through its own internalization pathway. The theory also shows how competition from metal complexes can significantly modify the uptake flux of free metals. The impact of this competition is determined not only by its nature (competitive, uncompetitive, noncompetitive, or mixed competitive inhibition), but also by the lability of the complexed metal species (when operative), and the specific uptake characteristics of both free and complexed metals, as determined by their respective Bosma numbers (diffusion- or absorption-limited biouptake). The comprehensive theory developed herein offers an alternative to the traditional and often restrictive BLM, for interpreting bioaccumulation data and testing the applicability of different internalization mechanisms. Unlike BLM, which is merely a specific situation covered by the model, our framework can quantitatively access the contribution, if any, of metal complexes to biouptake. These benefits are illustrated by analyzing existing literature data[27] on the biouptake of neodymium by *Chlamydomonas reinhardtii*.

Overall, this work presents a rigorous and thorough theoretical framework for predicting metal bioaccumulation in aquatic environments, moving beyond the popular equilibrium-based view of metal bioavailability. Refinements of this framework include accounting for metal depletion from the bulk solution during bioaccumulation,[14] analyzing speciation situations that involve multidentate species and ligand mixtures,[54−57] and integrating the lability of metal complexes when the ligand is a colloid or a nanoparticle.[16−18,58−60] We also anticipate that the biouptake flux expressions derived herein will be valuable for interpreting the bioaccumulation and/or bioremoval of emerging metallic contaminants, such as rare earth metals, or for more accurately defining metal toxicity thresholds in risk assessment.[61−67] For the sake of example, our model, unlike standard BLM, can quantitatively predict an increase in metal uptake in the presence of ligands. This is a phenomenon that has been documented in the scientific literature,[33,47−50,67−69] and our model offers several scenarios that are consistent with this non-BLM behavior.

■ ASSOCIATED CONTENT

Supporting Information

The Supporting Information is available free of charge at https://pubs.acs.org/doi/10.1021/acsenvironau.5c00293.

Details on the derivation of eq 3 (SI-A), the expression of the dimensionless uptake flux $Q_{i=M,ML}$ in the linear Henry regime when M and ML are taken up by distinct diffusion-facilitated pathways (SI-B), and Figure S1 shows the variations of Q_{ML} under the conditions of Figure 9E,F (SI-C) (PDF)

■ AUTHOR INFORMATION

Corresponding Author

Jérôme F. L. Duval − *CNRS, LIEC, Université de Lorraine, Nancy F-54000, France;* orcid.org/0000-0002-5458-3761; Email: jerome.duval@univ-lorraine.fr

Authors

Herman P. van Leeuwen − *ECOSPHERE, Department of Biology, Universiteit Antwerpen, Antwerpen 2020, Belgium*

Raewyn M. Town − *ECOSPHERE, Department of Biology, Universiteit Antwerpen, Antwerpen 2020, Belgium;* orcid.org/0000-0001-9505-1465

Complete contact information is available at: https://pubs.acs.org/10.1021/acsenvironau.5c00293

Author Contributions

CRediT: **Jérôme F.L. Duval** conceptualization, data curation, formal analysis, investigation, methodology, resources, software, validation, visualization, writing - original draft, writing -

https://doi.org/10.1021/acsenvironau.5c00293
ACS Environ. Au XXXX, XXX, XXX−XXX

review & editing; **Herman P. van Leeuwen** investigation, writing - review & editing; **Raewyn M. Town** data curation, formal analysis, funding acquisition, investigation, validation, writing - original draft, writing - review & editing.

Notes

The authors declare no competing financial interest.

■ ACKNOWLEDGMENTS

RMT performed this work in the framework of the QTOX MSCA doctoral network funded by the European Union's Horizon Europe Research and Innovation program under the Marie Skłodowska-Curie Action Grant Agreement 101072531.

■ GLOSSARY (MAIN SYMBOLS)

Latin

$A_{0,1,2}$ and $B_{0,1,2}$	Dimensionless coefficients involved in the polynomial expressions defining the dimensionless M and ML surface concentrations (cf. Table 1 and Section 3.3.2).
a	Cell radius (m)
$a_{i=\mathrm{M,ML}}$	Dimensionless M and ML bioaffinity parameters, defined by the ratios $K_{\mathrm{u},i=\mathrm{M,ML}}/c^*_{i=\mathrm{M,ML}}$.
$b_{i=\mathrm{M,ML}}$	Dimensionless M and ML bioconversion capacities, defined by the ratios $J^{\max}_{\mathrm{u},i=\mathrm{M,ML}}/(pJ^{\max}_{\mathrm{Diff},i=\mathrm{M,ML}})$.
$Bn_{i=\mathrm{M,ML}}$	M and ML Bosma numbers (dimensionless) defined by eqs 14 and 20, respectively.
$c^*_{i=\mathrm{M,L,ML}}$	Concentrations of M, L and ML in bulk solution (mol m^{-3}).
$D_{i=\mathrm{M,ML}}$	Diffusion coefficient of M and ML (m^2 s^{-1}).
$J^{\max}_{\mathrm{Diff},i=\mathrm{M,ML}}$	Maximum M and ML diffusion flux from solution to the metal-bioaccumulating surface (mol m^2 s^{-1}), defined by $J^{\max}_{\mathrm{Diff},i=\mathrm{M,ML}} = D_{i=\mathrm{M,ML}}c^*_{i=\mathrm{M,ML}}/a$ (uncorrected for stirring in solution, cf. caption Figure 11).
$J_{i=\mathrm{M,ML}}$	Diffusion supply flux of M and ML at the metal-bioaccumulating surface (mol m^2 s^{-1}).
$J_{\mathrm{u},i=\mathrm{M,ML}}$	Internalization (or uptake) flux of M and ML (mol m^2 s^{-1}).
$J^{\max}_{\mathrm{u},i=\mathrm{M,ML}}$	Maximum internalization flux of M and ML defined by $J^{\max}_{\mathrm{u},i=\mathrm{M,ML}} = K_{\mathrm{H},i=\mathrm{M,ML}}k_{\mathrm{int},i=\mathrm{M,ML}}K_{\mathrm{u},i=\mathrm{M,ML}}$ (mol m^2 s^{-1}).
$k_{\mathrm{a,d}}$	Kinetic constants for ML formation (k_{a}, m^3 mol^{-1} s^{-1}) and dissociation (k_{d}, s^{-1}).
$k_{\mathrm{int},i=\mathrm{M,ML}}$	Kinetic constants for M and ML internalization (s^{-1}).
$K_{\mathrm{ML}} = c^*_{\mathrm{ML}}/(c^*_{\mathrm{L}}c^*_{\mathrm{M}})$	Metal complexation constant or, equivalently, ML stability constant (m^3 mol^{-1}).
$\overline{K}_{\mathrm{ML}} = K_{\mathrm{ML}}c^*_{\mathrm{L}}$	Dimensionless metal complexation constant.
$K_{\mathrm{u},i=\mathrm{M,ML}}$	M and ML half-saturation constants (mol m^{-3}), corresponding to the reciprocal of the stability constants (m^3 mol^{-1}) that describe the M and ML binding with their respective active transporter sites.
$K^{(1)}_{i=\mathrm{M,ML}}$	Reciprocals of the stability constants that describe the binding of M and ML with the nonactive (inhibitory) sites of the protein transporters (mol m^{-3}).
p	Defined by $p = 1 + \varepsilon\overline{K}_{\mathrm{ML}}\xi$ (dimensionless).
$Q_{i=\mathrm{M,ML}}$	Dimensionless uptake flux of M and ML, defined by $Q_{i=\mathrm{M,ML}} = J_{\mathrm{u},i=\mathrm{M,ML}}/J^{\max}_{\mathrm{u},i=\mathrm{M,ML}}$.
Q_{T}	Total dimensionless metal uptake flux defined by eq 41.
$x = \overline{c}^{(\mathrm{a})}_{\mathrm{M}}$	Dimensionless M concentration at the metal bioaccumulating surface defined by $x = c_{\mathrm{M}}(\overline{r} = 1)/c^*_{\mathrm{M}}$, where $c_{\mathrm{M}}(\overline{r} = 1)$ correspond to the surface concentration of M.
$y = \overline{c}^{(\mathrm{a})}_{\mathrm{ML}}$	Dimensionless ML concentration at the metal bioaccumulating surface defined by $y = c_{\mathrm{ML}}(\overline{r} = 1)/c^*_{\mathrm{ML}}$, where $c_{\mathrm{ML}}(\overline{r} = 1)$ correspond to the surface concentration of ML.

Greek

β_{ML}	Diffusion conductance ratio defined by eq 28 (dimensionless).
$\gamma_{i=\mathrm{M,ML}}$	Dimensionless constants defined by eq 7.
δ_{o}	Membrane thickness involved in eq 25 (m).
δ	Diffusion layer thickness (m) in moderately stirred solution (cf. caption of Table 2).
$\varepsilon = D_{\mathrm{ML}}/D_{\mathrm{M}}$	ML to M diffusion coefficients ratio (dimensionless).
η	Dimensionless scalar defined by $\eta = J^{\max}_{\mathrm{Diff,ML}}/J^{\max}_{\mathrm{Diff,M}} = \varepsilon\overline{K}_{\mathrm{ML}}$.
$\overline{\kappa}_{\mathrm{a}} = k_{\mathrm{a}}a^2c^*_{\mathrm{L}}/D_{\mathrm{M}}$	Dimensionless Damkhöler number comparing the time scale of M diffusion, a^2/D_{M}, and the ML formation time scale, $1/(k_{\mathrm{a}}c^*_{\mathrm{L}})$.
ξ	ML lability, defined by eq 13 (dimensionless).
ψ	Defined by eq 24.

■ REFERENCES

(1) Poldoski, J. E. Cadmium bioaccumulation assays − their relationship to various ionic equilibria in Lake Superior water. *Environ. Sci. Technol.* **1979**, *13*, 701−706.

(2) Zhao, C.-M.; Campbell, P. G. C.; Wilkinson, K. J. When are metal complexes bioavailable? *Environ. Chem.* **2016**, *13*, 425−433.

(3) van Leeuwen, H. P. Metal speciation dynamics and bioavailability: inert and labile complexes. *Environ. Sci. Technol.* **1999**, *33*, 3743−3748.

(4) Duval, J. F. L.; van Leeuwen, H. P.; Town, R. M. Electrostatic effects on ligand-assisted transfer of metals to (bio)accumulating interfaces and metal complexes (bioavai)lability. *Colloids Surf. A: Physicochem. Eng. Asp.* **2023**, *658*, No. 130679.

(5) Di Toro, D. M.; Allen, H. E.; Bergman, H. L.; Meyer, J. S.; Paquin, P. R.; Santore, R. C. A biotic ligand model of the acute toxicity of metals. 1. Technical basis. *Environ. Toxicol. Chem.* **2001**, *20*, 2383−2396.

(6) Paquin, P. R.; Gorsuch, J. W.; Apte, S.; Batley, G. E.; Bowles, K. C.; Campbell, P. G. C.; Delos, C. G.; Di Toro, D. M.; Dwyer, R. L.; Galvez, F.; Gensemer, R. W.; Goss, G. G.; Hogstrand, C.; Janssen, C. R.; McGeer, J. C.; Naddy, R. B.; Playle, R. C.; Santore, R. C.; Schneider, U.; Stubblefield, W. A.; Wood, C. M.; Wu, K. B. The biotic ligand model: a historical overview. *Compar. Biochem. Physiol. C* **2002**, *133*, 3−35.

https://doi.org/10.1021/acsenvironau.5c00293
ACS Environ. Au XXXX, XXX, XXX−XXX

(7) Town, R. M.; van Leeuwen, H. P.; Duval, J. F. L. Rigorous physicochemical framework for metal ion binding by aqueous nanoparticulate humic substances: implications for speciation modeling by the NICA-Donnan and WHAM codes. *Environ. Sci. Technol.* **2019**, *53*, 8516−8532.
(8) Nyarko, L.; Dewey, C.; Nason, J. A.; Boiteau, R. M. Tracking changes in organic-copper speciation during wastewater treatment using LC-ICPMS-ESIMS. *ACS Environ. Au* **2025**, *5*, 230−240.
(9) Al Harraq, A.; Brahana, P. J.; Arcemont, O.; Zhang, D.; Valsaraj, K. T.; Bharti, B. Effects of weathering on microplastic dispersibility and pollutant uptake capacity. *ACS Environ. Au* **2022**, *2*, 549−555.
(10) Carnamucio, F.; Foti, C.; Saija, F.; Cassone, G.; Giuffrè, O. Speciation and thermodynamic study of arsenic(III)-pharmaceutical complexes in aqueous solutions. *ACS Environ. Au* **2025**, *5*, 404−414.
(11) Jansen, S.; Blust, R.; van Leeuwen, H. P. Metal speciation dynamics and bioavailability: Zn(II) and Cd(I) uptake by mussel (*Mytilus edulis*) and carp (*Cyprinus carpio*). *Environ. Sci. Technol.* **2002**, *36*, 2164−2170.
(12) Duval, J. F. L. Coupled metal partitioning dynamics and toxicodynamics at biointerfaces: a theory beyond the biotic ligand model framework. *Phys. Chem. Chem. Phys.* **2016**, *18*, 9453−9469.
(13) Duval, J. F. L.; Présent, R. M.; Rotureau, E. Kinetic and thermodynamic determinants of trace metal partitioning at bio-interphases: the role of intracellular speciation dynamics. *Phys. Chem. Chem. Phys.* **2016**, *18*, 30415−30435.
(14) Duval, J. F. L. Dynamics of metal uptake by charged biointerphases: bioavailability and bulk depletion. *Phys. Chem. Chem. Phys.* **2013**, *15*, 7873−7888.
(15) Duval, J. F. L.; Rotureau, E. Dynamics of metal uptake by charged soft biointerphases: impacts of depletion, internalisation, adsorption and excretion. *Phys. Chem. Chem. Phys.* **2014**, *16*, 7401−7416.
(16) van Leeuwen, H. P.; Duval, J. F. L.; Pinheiro, J. P.; Blust, R.; Town, R. M. Chemodynamics and bioavailability of metal ion complexes with nanoparticles in aqueous media. *Environ. Sci.: Nano* **2017**, *4*, 2108−2133.
(17) Duval, J. F. L.; Town, R. M.; van Leeuwen, H. P. Lability of nanoparticulate metal complexes at a macroscopic metal responsive (bio)interface: expression and asymptotic scaling laws. *J. Phys. Chem. C* **2018**, *122*, 6052−6065.
(18) Duval, J. F. L. Chemodynamics of metal ion complexation by charged nanoparticles: a dimensionless rationale for soft, core-shell and hard particle types. *Phys. Chem. Chem. Phys.* **2017**, *19*, 11802−11815.
(19) Peters, A.; Merrington, G.; Schlekat, C.; De Schamphelaere, K.; Stauber, J.; Batley, G.; Harford, A.; van Dam, R.; Pease, C.; Mooney, T.; Warne, M.; Hickey, C.; Glazebrook, P.; Chapman, J.; Smith, R.; Krassoi, R. Validation of the nickel biotic ligand model for locally relevant species in Australian freshwaters. *Environ. Toxicol. Chem.* **2018**, *37*, 2566−2574.
(20) Liang, W.; Zhao, X.; Wang, X.; Tang, Z.; Zhang, X.; Wang, X. Application of multiple linear regression models in deriving water quality criteria for lead: comparison of metal bioavailability estimation approaches. *ACS EST Water* **2024**, *4*, 5290−5300.
(21) Mebane, C. A. Bioavailability and toxicity models of copper to freshwater life: the state of regulatory science. *Environ. Toxicol. Chem.* **2023**, *42*, 2529−2563.
(22) Michaelis, L.; Menten, M. L. Die Kinetik der Invertinwirkung. *Biochemische Zeitschrift* **1913**, *49*, 333−369.
(23) Handy, R. D.; Musonda, M. M.; Phillips, C.; Falla, S. J. Mechanisms of gastrointestinal copper absorption in the African walking catfish: copper dose-effects and a novel anion-dependent pathway in the intestine. *J. Exp. Biol.* **2000**, *203*, 2365−2377.
(24) Ibrahim, M.; Minghetti, M. Effect of chloride concentration on the cytotoxicity, bioavailability, and bioreactivity of copper and silver in the rainbow trout gut cell line, RTgutGC. *Ecotoxicology* **2022**, *31*, 626−636.
(25) Nebert, D. W.; Gálvez-Peralta, M.; Ben Hay, E.; Li, H.; Johansson, E.; Yin, C.; Wang, B.; He, L.; Soleimani, M. ZIP14 and ZIP8 zinc/bicarbonate symporters in *Xenopus* oocytes: characterization of metal uptake and inhibition. *Metallomics* **2012**, *4*, 1218−1225.
(26) Jiang, Y.; Li, Z.; Sui, D.; Sharma, G.; Wang, T.; MacRenaris, K.; Takahashi, H.; Merz, K.; Hu, J. Rational engineering of an elevator-type metal transporter ZIP8 reveals a conditional selectivity filter critically involved in determining substrate specificity. *Commun. Biol.* **2023**, *6*, No. 778.
(27) Yang, G.; Wilkinson, K. J. Biouptake of a rare earth metal (Nd) by *Chlamydomonas reinhardtii* - Bioavailability of small organic complexes and role of hardness ions. *Environ. Pollut.* **2018**, *243*, 263−269.
(28) Tjälve, H.; Gottofrey, J. Effects of lipophilic complex formation on the uptake and distribution of some metals in fish. *Pharmacol. Toxicol.* **1991**, *69*, 430−439.
(29) Boullemant, A.; Lavoie, M.; Fortin, C.; Campbell, P. G. C. Uptake of hydrophobic metal complexes by three freshwater algae: unexpected influence of pH. *Environ. Sci. Technol.* **2009**, *43*, 3308−3314.
(30) Errecalde, O.; Seidl, M.; Campbell, P. G. C. Influence of a low-molecular-weight metabolite (citrate) on the toxicity of cadmium and zinc to the unicellular green alga *Selenastrum capricornutum*: an exception to the free-ion model. *Water Res.* **1998**, *32*, 419−429.
(31) Fortin, C.; Campbell, P. G. C. Thiosulfate enhances silver uptake by a green alga: role of anion transporters in metal uptake. *Environ. Sci. Technol.* **2001**, *35*, 2214−2218.
(32) Cremazy, A.; Campbell, P. G. C.; Fortin, C. In the presence of fluoride, free Sc^{3+} is not a good predictor of Sc bioaccumulation by two unicellular algae: possible role of fluorocomplexes. *Environ. Sci. Technol.* **2014**, *48*, 9754−9761.
(33) Meylan, S.; Behra, R.; Sigg, L. Influence of metal speciation in natural freshwater on bioaccumulation of copper and zinc in periphyton: a microcosm study. *Environ. Sci. Technol.* **2004**, *38*, 3104−3111.
(34) Hudson, R. J. M.; Morel, F. M. M. Iron transport in marine phytoplankton: kinetics of cellular and medium coordination reactions. *Limnol. Oceanogr.* **1990**, *35*, 1002−1020.
(35) Duval, J. F. L.; Maffei, L.; Delatour, E.; Zaffino, M.; Pagnout, C. Kinetics of metal detection by luminescence-based whole-cell biosensors: connecting biosensor response to metal bioavailability, speciation and cell metabolism. *Phys. Chem. Chem. Phys.* **2023**, *25*, 30276−30295.
(36) Duval, J. F. L.; Paquet, N.; Lavoie, M.; Fortin, C. Dynamics of metal partitioning at the cell-solution interface: Implications for toxicity assessment under growth-inhibiting conditions. *Environ. Sci. Technol.* **2015**, *49*, 6625−6636.
(37) Voet, D.; Voet, J. G.; Pratt, C. W. Fundamentals of biochemistry − life at the molecular level, 4th ed.; John Wiley & Sons, Inc.: Hoboken, NJ; Part III Enzymes, Chapter 12, Enzyme kinetics, Inhibition, and Control; p 355.
(38) Galceran, J.; Puy, J.; Salvador, J.; Cecilia, J.; van Leeuwen, H. P. Voltammetric lability of metal complexes at spherical microelectrodes with various radii. *J. Electroanal. Chem.* **2001**, *505*, 85−94.
(39) Best, J. B. The inference of intracellular enzymatic properties from kinetic data obtained on living cells. I. Some kinetic considerations regarding an enzyme enclosed by a diffusion barrier. *J. Cell Comp. Physiol.* **1955**, *46*, 1−27.
(40) Koch, A. L. Diffusion: The crucial process in many aspects of the biology of bacteria. *Adv. Microb. Ecol.* **1990**, *11*, 37−70.
(41) Bosma, T. N. P.; Middeldorp, P. J. M.; Schraa, G.; Zhender, A. J. B. Mass transfer limitation of biotransformation: quantifying bioavailability. *Environ. Sci. Technol.* **1997**, *31*, 248−252.
(42) Nelson, C. L.; Cox, M. M.; Hoskins, A. A. *Lehninger principles of biochemistry*. 8th ed.; Macmillan Learning: New York, 2021.
(43) Town, R. M.; van Leeuwen, H. P.; Duval, J. F. L. Effect of polymer aging on uptake/release kinetics of metal ions and organic molecules by micro- and nanoplastics: implications for the bioavailability of the associated compounds. *Environ. Sci. Technol.* **2023**, *57*, 16552−16563.

https://doi.org/10.1021/acsenvironau.5c00293
ACS Environ. Au XXXX, XXX, XXX−XXX

(44) Levich, V. G. *Physicochemical Hydrodynamics*; Scripta Technica Inc.: Englewood Cliffs, NJ, 1962.
(45) van Leeuwen, H. P.; Pinheiro, J.-P. Lability criteria for metal complexes in micro-electrode voltammetry. *J. Electroanal. Chem.* **1999**, *471*, 55−61.
(46) Tan, Q.-G.; Yang, G.; Wilkinson, K. J. Biotic ligand model explains the effects of competition but not complexation for Sm biouptake by *Chlamydomonas reinhardtii*. *Chemosphere* **2017**, *168*, 426−434.
(47) Yang, G.; Tan, Q.-G.; Zhu, L.; Wilkinson, K. J. The role of complexation and competition in the biouptake of europium by a unicellular alga. *Environ. Toxicol. Chem.* **2014**, *33*, 2609−2615.
(48) Wilkinson, K. J.; Campbell, P. G. C.; Couture, P. Effect of fluoride complexation on aluminum toxicity towards juvenile Atlantic salmon (*Salmo salar*). *Can. J. Fish. Aquat. Sci.* **1990**, *47*, 1446−1452.
(49) Zhao, C.-M.; Wilkinson, K. J. Biotic ligand model does not predict the bioavailability of rare earth elements in the presence of organic ligands. *Environ. Sci. Technol.* **2015**, *49*, 2207−2214.
(50) Sánchez-Marín, P.; Liu, F.; Chen, Z.; Fortin, C.; Campbell, P. G. C. Microalgal-driven pH changes in the boundary layer lead to apparent increases in Pb internalization by a unicellular alga in the presence of citrate. *Limnol. Oceanogr.* **2018**, *63*, 1328−1339.
(51) Slaveykova, V. I.; Wilkinson, K. J.; Ceresa, A.; Pretsch, E. Role of fulvic acid on lead bioaccumulation by *Chlorella kesslerii*. *Environ. Sci. Technol.* **2003**, *37*, 1114−1121.
(52) Gustafsson, J. P. *Visual MINTEQ. Version 4.0*; KTH Royal Institute of Technology: Stockholm, Sweden, 2024. https://vminteq.com/.
(53) Li, Y.-H.; Gregory, S. Diffusion of ions in sea water and in deep-sea sediments. *Geochim. Cosmochim. Acta* **1974**, *38*, 703−714.
(54) Puy, J.; Cecilia, J.; Galceran, J.; Town, R. M.; van Leeuwen, H. P. Voltammetric lability of multiligand complexes. The case of ML_2. *J. Electroanal. Chem.* **2004**, *571*, 121−132.
(55) Komuro, T.; Nakajima, Y.; Takaya, J.; Hashimoto, H. Recent progress in transition metal complexes supported by multidentate ligands featuring group 13 and 14 elements as coordinating atoms. *Coord. Chem. Rev.* **2022**, *473*, No. 214837.
(56) Mota, A. M.; Pinheiro, J. P.; Simões Gonçalves, M. L. Electrochemical methods for speciation of trace elements in marine waters. *Dynamic aspects. J. Phys. Chem. A* **2012**, *116*, 6433−6442.
(57) Zhang, Z.; Alemani, D.; Buffle, J.; Town, R. M.; Wilkinson, K. J. Metal flux through consuming interfaces in ligand mixtures: boundary conditions do not influence the lability and relative contributions of metal species. *Phys. Chem. Chem. Phys.* **2011**, *13*, 17606−17614.
(58) Duval, J. F. L.; Town, R. M.; van Leeuwen, H. P. Applicability of the reaction layer principle to nanoparticulate metal complexes at a macroscopic reactive (bio)interface: a theoretical study. *J. Phys. Chem. C* **2017**, *121*, 19147−19161.
(59) Gopmandal, P. P.; Duval, J. F. L. Electrostatics and electrophoresis of engineered nanoparticles and particulate environmental contaminants: beyond zeta potential-based formulation. *Curr. Opin. Colloid Interface Sci.* **2022**, *60*, No. 101605.
(60) Duval, J. F. L.; van Leeuwen, H. P. Rates of ionic reactions with charged nanoparticles in aqueous media. *J. Phys. Chem. A* **2012**, *116*, 6443−6451.
(61) Chormare, R.; Anil Kumar, M. Environmental health and risk assessment metrics with special mention to biotransfer, bioaccumulation and biomagnification of environmental pollutants. *Chemosphere* **2022**, *302*, No. 134836.
(62) Lachaux, N.; Cossu-Leguille, C.; Poirier, L.; Gross, E. M.; Giamberini, L. Integrated environmental risk assessment of rare earth elements mixture on aquatic ecosystems. *Front. Environ. Sci.* **2022**, *10*, No. 974191.
(63) Singh, A.; Čížková, M.; Náhlík, V.; Mezricky, D.; Schild, D.; Rucki, M.; Vítová, M. Bio-removal of rare earth elements from hazardous industrial waste of CFL bulbs by the extremophile red alga *Galdieria sulphuraria*. *Front. Microbiol.* **2023**, *14*, No. 5650.
(64) Sun, Y.; Lu, T.; Pan, Y.; Shi, M.; Ding, D.; Ma, Z.; Liu, J.; Yuan, Y.; Fei, L.; Sun, Y. Recovering rare earth elements via immobilized red algae from ammonium-rich wastewater. *Env. Sci. Ecotechnol.* **2022**, *12*, No. 100204.
(65) Kohl, J.; Schweikert, M.; Klass, N.; Lemloh, M.-L. Intracellular bioaccumulation of the rare earth element Gadolinium in ciliate cells resulting in biogenic particle formation and excretion. *Sci. Rep.* **2023**, *13*, 5650.
(66) Revel, M.; van Drimmelen, C. K. E.; Weltje, L.; Hursthouse, A.; Heise, S. Effects of rare earth elements in the aquatic environment: implications for ecotoxicological testing. *Crit. Rev. Environ. Sci. Technol.* **2025**, *55*, 334−375.
(67) Houtarné, O.; Scott Smith, D.; Fortin, C. Natural organic matter (NOM) can increase the uptake fluxes of three critical metals (Ga, La, Pt) in a unicellular green alga. *Chemosphere* **2024**, *365*, No. 143311.
(68) Degryse, F.; Smolders, E.; Merckx, R. Labile Cd complexes increase Cd availability to plants. *Environ. Sci. Technol.* **2008**, *40*, 830−836.
(69) Ytreberg, E.; Karlsson, J.; Hoppe, S.; Eklund, B.; Ndungu, K. Effect of organic complexation on copper accumulation and toxicity to the estuarine red macroalga *Ceramium tenuicorne*: a test of the free ion activity model. *Environ. Sci. Technol.* **2011**, *45*, 3145−3153.

https://doi.org/10.1021/acsenvironau.5c00293
ACS Environ. Au XXXX, XXX, XXX−XXX